NGU REPORT 2023.026

Trenching and 14C dating of the Stuoragurra Fault Complex in Finnmark, Northern Norway, and geohazard implications

GEOLOGY FOR SOCIETY

SINCE 1858

GEOLOGICAL SURVEY OF NORWAY

- NGU -

NGU REPORT

2023.026

Trenching and ^{14}C dating of the Stuoragurra Fault Complex in Finnmark, Northern Norway, and geohazard implications

Trenching transverse to the 2 m high fault scarp at Borgagurra, Stuoragurra Fault Complex, Finnmark, Northern Norway, 2023. Machine driver: Per Edvard Johnsen.

NORGES GEOLOGISKE UNDERSØKELSE
- NGU -

REPORT

Geological Survey of Norway
P.O.Box 6315 Torgarden
NO-7491 TRONDHEIM
Tel.: 47 73 90 40 00

Report no.: 2023.026	ISSN: 0800-3416 (print) ISSN: 2387-3515 (online)	Grading: Open

Title:
Trenching and ^{14}C dating of the postglacial Stuoragurra Fault Complex in Finnmark, Northern Norway, and geohazard implications

Authors:	**Client:**
Olsen, L. & Olesen, O.	NGU, Kartverket, OD, UiB, Equinor, OKEA

County:	**Commune:**
Finnmark (Troms & Finnmark)	Kautokeino, Karasjok, Alta, Porsanger
Map-sheet name (M=1:250.000)	**Map-sheet no. and -name (M=1:50.000)**
Karasjok, Nordreisa	1933 IV, 1934 I, II, III, 2034 IV,
Deposit name and grid-reference:	**Number of pages:** 63 **Price (NOK):** 205.-

Fieldwork carried out:	**Date of report:**	**Project no.:**	**Person responsible:**
2018-2023	30.11.2023	404400	Marco Brönner

Summary:
The Stuoragurra Fault Complex (SFC) constitutes the Norwegian part of the larger Lapland Province of postglacial faults in northern Fennoscandia. The 90 km long SFC consists of two separate fault systems: the Máze Fault (revised) System in the southwestern area and the Iešjávri Fault System to the northeast. The distance between the fault systems is 12 km. The faults dip at an angle of 30–75° to the SE. Here we present data from trenching of different fault sections. The trenching reveals deformed overburden in all 11 sites and inclusions of peat and organic bearing soil in the deformed and partly overrun loose deposits on the footwall in most of the sites. Radiocarbon dating of macro remains of plants located in buried and severely deformed sediment horizons indicates late Holocene ages for the (final) formation of the different fault segments, more specifically that the faulting at Fitnajohka and Máze in the Máze Fault System formed during earthquakes younger than c. 470-500 years ago. The thickness of the deformed part of the total Holocene peat thickness (c. 2.4 m of 2.6 m) is consistent with a young faulting age. The youngest age, between c. 330 and 500 years ago, or possibly less than 380 years ago, is recorded at Juovssajávrrit in the Iešjávri Fault System in the northeast. Plant macrofossil data from the buried and deformed sediments at Máze suggest an early to late Holocene vegetation cover, and thereby also implying that the faulting is of late postglacial age there. The maximum reverse displacement of c. 9 m and fault system length of 42 km of the Máze Fault System indicate both a moment magnitude of c. 6.9 on Richter's scale if just one rupture event is associated with the segments of this system. Similar data for the Iešjávri Fault System (maximum 4 m reverse displacement and a total length of 34 km) indicate an associated earthquake of magnitude c. 6.8. The fault rupture with length and height of fault scarps, and injections and throw-out of angular boulders and wedges of unconsolidated fault breccia reaching up to 15–20 m away from the fault scarp give the most distinct expressions of the associated earthquake magnitude. Recorded landslides and rock avalanches in or close to the SFC indicate a possible link to strong earthquakes along the fault complex as a triggering mechanism during the Holocene. The exceptionally young ages of the Máze and Iešjávri fault systems imply a need to study the geohazard implications. It is for instance necessary to date more carefully both the Nordmannvikdalen postglacial fault and numerous rock avalanches in the North Troms area that have previously been assumed to be of Younger Dryas age.

Keywords: Postglacial fault	Reverse fault	Neotectonics
^{14}C dating	Sediment deformation	Macro plant remains
Fault breccia	Landslide	Rock avalanche

Content

28 figures

4 tables

This report is an updated version of an earlier report (Olsen et al., 2022), with new field data from 2022-2023, accompanying dates and discussion.

Corresponding authors: Lars Olsen (Lars.Olsen@ngu.no) vs. trenching and ^{14}C dating; Odleiv Olesen (Odleiv.Olesen@ngu.no) vs. project management, geophysics, bedrock geology and map production.

Introduction

Two postglacial faults have previously been reported from Norway: The Nordmannvikdalen Fault, i.e., a normal fault in northern Troms (Bakken, 1983; Tolgensbakk & Sollid, 1988; Dehls et al., 2000; Olsen et al., 2018), and the Stuoragurra Fault Complex (SFC), the latter comprising at least 29 reverse fault segments in western Finnmark (Olesen, 1988; Olesen et al., 1992a, b, 2004, 2013, 2021; Bungum & Lindholm, 1997; Roberts et al., 1997; Dehls et al., 2000;). The faults have been assumed to be of Younger Dryas and postglacial age, respectively, and constitute the northern part of the Lapland Postglacial Fault Province in northern Fennoscandia (Lagerbäck & Sundh, 2008; Olesen et al., 2013; Smith et al., 2014; Sutinen et al., 2014; Mikko et al., 2015; Palmu et al., 2015). The postglacial faults are assumed to have formed because of released excess horizontal stresses generated during glaciation and activated by deglaciation and glacial isostatic rebound (Wu et al., 1999; Lund et al., 2009; Steffen et al., 2014a, b). Lagerbäck & Sundh (2008) argue further that the outburst of lateglacial faulting in northern Sweden was restricted to the last deglaciation. They argued that the modest glacial erosion in this part of Sweden would allow older fault scarps of similar magnitude to be preserved, and such older fault scarps have not been reported. The postglacial faults in northern Fennoscandia (Fig. 1) have been considered to represent single rupture events at the end of, or after, the last Weichselian glaciation. Lagerbäck & Sundh (2008), Smith et al. (2018) and Mattila et al. (2019) have, however, provided field evidence for multiple slip events, some of these probably older than postglacial time, and some represent postglacial faulting.

A review of the present-day knowledge of the structure and deformation along the postglacial SFC was given by Olesen et al. (2021), and their main conclusions were also included as background information in a report focused on trenching and dating of the SFC (Olsen et al. 2022). The latter presented merely a compilation of the results from analyses of aerial photographs, LIDAR data and trenching across fault scarps of the Stuoragurra Fault Complex, including radiocarbon dating and macrofossil content of buried organic material, geophysical profiling, and K-Ar dating and XRD and XRF analysis of a sample of fault gouge from Ellajávri, south-southwest of Máze. The ^{14}C dating results indicate late postglacial ages of the youngest fault events, however with possibly different ages in the separate faults systems of the SFC.

Olesen et al. (2021) grouped the SFC segments into the Fitnajohka, Máze and Iešjávri Fault Systems, which was also used by Olsen et al. (2022). However, new trenching and dating last year have led to a revision of this, with just one major rupture event in the southern and

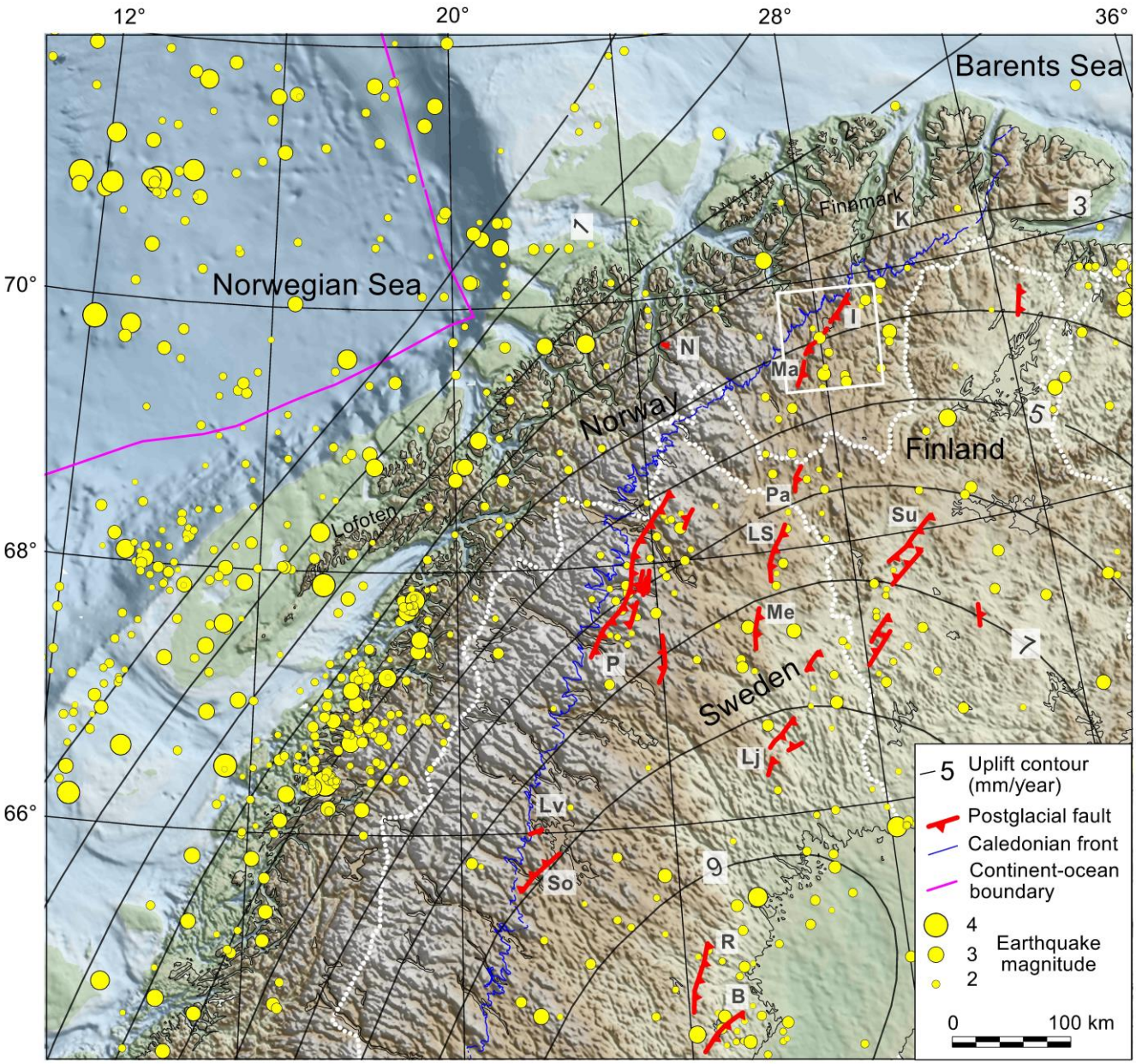

Fig. 1. Postglacial faults, topography, bathymetry, earthquakes during the period 1750–2011 and present-day uplift (mm/year) in northern and central Fennoscandia (modified from Olesen et al., 2021). The Norwegian National Seismological Network at the University of Bergen is the source of the earthquake data in Norway, Svalbard and NE Atlantic. Data on the other earthquakes in Finland and Sweden are downloaded, from the web pages of the Institute of Seismology at the University of Helsinki; http://www.seismo.helsinki.fi/english/bulletins/index.html. The topography and bathymetry are compiled from various sources by Olesen et al. (2010). Most of the faults within the Lapland province of postglacial faults cuts the present-day uplift contours at an angle of 30-70°. The postglacial faults occur in areas with increased seismicity indicating that they are active at depth. The Stuoragurra, Pärvie, Laisvall and Sorsele Faults are located immediately to the east of the Caledonian front. The black frame shows the location of Figs. 2 and 3 and the Stuoragurra Fault Complex. N- Nordmannvikdalen Fault; I and Ma- Iešjávri and Máze fault systems in the Stuoragurra Fault Complex; B- Burträsk Fault; Lj- Lansjärv Fault; LS- Lainio-Suijavaara Fault; Lv- Laisvall Fault; Me- Merasjärvi Fault; P- Pärvie Fault; Pa- Palojärvi; Fault; R- Röjnoret Fault; So- Sorsele Fault; Su- Suasselkä Fault. K- Kunes, i.e., approximate position of a rock avalanche in the NE.

middle area, suggesting a combination of the two former systems there to just one. The present model describes the SFC to be represented by the Máze (revised) and Iešjávri Fault Systems (Figs. 2 & 3).

Lithified fault breccia has been recorded in bedrock in the fault zone at Fitnajohka (Olesen et al., 1992a, Roberts et al., 1997), and in all trenches reaching bedrock. This indicates old fault activity with formation of fault breccia along the c. 4–8 km wide Proterozoic Mierojávri-Sværholt Shear Zone (MSSZ, Olesen et al., 1992a; Olesen & Sandstad, 1993; Mrope et al., in press) followed by a period (or periods) with diagenesis. Structural mapping by Henderson et al. (2015) has verified this interpretation. In addition, weathering of fault gouge at Fitnajohka, with production of, e.g., kaolinite and vermiculite (Åm, 1994) a long time before the youngest fault activity in the SFC zone, indicates together with the lithified breccia that the SFC is merely a postglacial reactivation of an old fault zone.

In this paper we present the overall data collected from trenching across fault scarps along the SFC and ^{14}C dating of macro plant remains in buried and deformed overburden sediments, interpretations of these and an evaluation of the significance of these for dating of the SFC.

In addition, magnitude of earthquakes associated with the formation of the SFC is considered based on fault length and scarp hight (Table 1), and one single rupture event in each system, after a model presented by Wells & Coppersmith (1994).

Fault/fault system	Length km	Number of segments	Trend	Maximum scarp height m	Height/ length	Estimated maximum displacement	Magnitude from fault length	Magnitude from max. displacement	Age cal. kyr BP
Nordmann-vikdalen	1.5	3	NW-SE	1.5	0.0010	2.3	6.0	6.6	11.5-0.5
Máze 1			NE-SW	2		3		6.7	<3.0
Máze 2	42	22 (?)	NE-SW	7	0.0002	9	6.9	6.9	<0.43
Iešjávri	34	9	NE-SW	3	0.0001	4	6.8	6.8	<0.43

Table 1. Summary of properties of postglacial faults in Norway. The major faults in the Precambrian of Finnmarksvidda are NE-SW trending and reverse. The Nordmannvikdalen fault in northern Troms is a smaller normal fault trending perpendicular to most of the reverse faults in northern Fennoscandia. The scarp height/length ratio is generally less than 0.001. Moment magnitudes are calculated from fault offset and length utilising formulas by Wells & Coppersmith (1994).

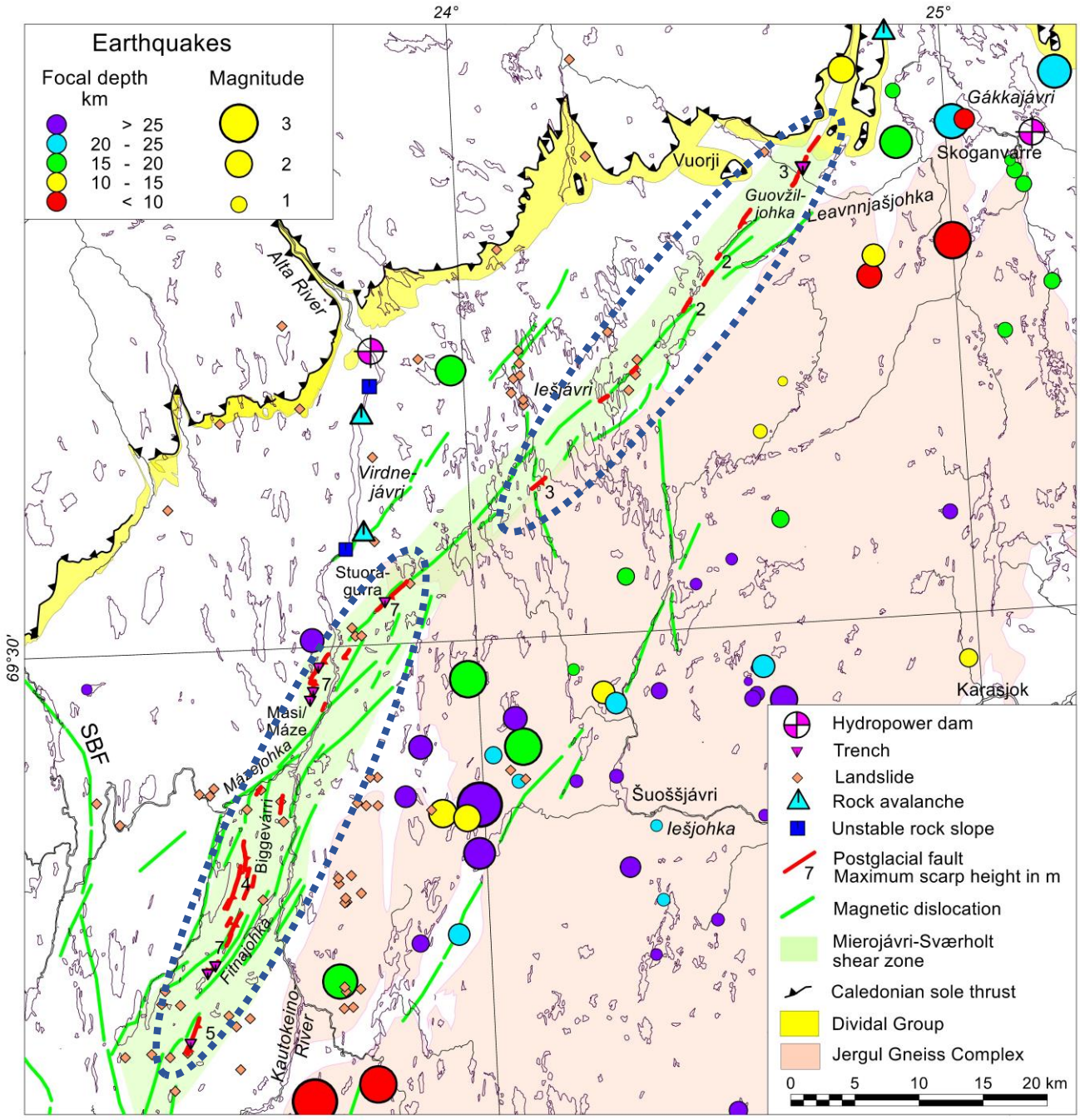

Fig. 2. Simplified geological map of the middle and northern parts of Finnmarksvidda (modified from Olesen et al. (2021). The 90 km long Stuoragurra Fault Complex (SFC) consists of two separate fault systems (*stiplet contours*); the Máze Fault System in the southern part and the Iešjávri Fault System to the northeast. The SFC occurs within the 4–5 km wide Mierojávri-Sværholt Shear Zone (MSSZ) that is located along the northwestern boundary of the Jergul Gneiss Complex (Olesen et al., 1992a). The MSSZ is also characterized by magnetic anomalies produced by the highly magnetic mafic intrusions (diabase, albite diabase and gabbro). An albite diabase south of Máze has been dated by Bingen et al. (2015) to 2220 ± 7 Ma. SBF – Soagŋojávri-Bajášjávri Fault (Olesen & Sandstad, 1993). Evidence of a total of 70 landslides is found within 20 km from the fault scarp. The earthquake epicentres are based on recordings at the ARCES seismic array immediately to the north of Karasjok in addition to seismic stations in northern Norway, and northern Finland.

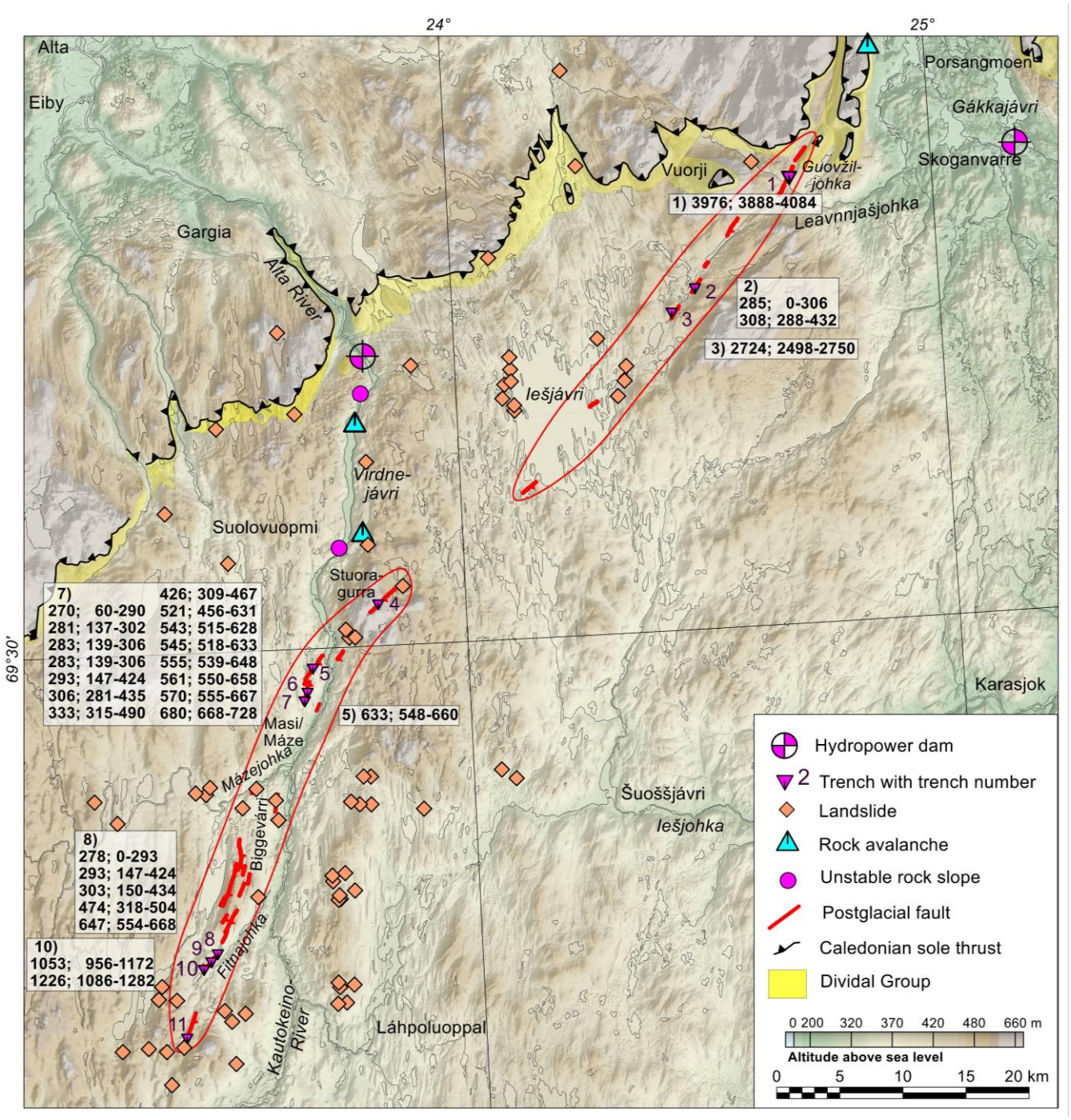

Fig. 3. The two fault systems (Máze in the south and Iešjávri in the north, red contours) of the SFC (red line segments) are separated with a 12 km long gap without faults, and are associated with earthquakes of 6.9 and 6.8, respectively, and may have different ages. Faulting in the Máze Fault System is dated to less than 430 cal. yr BP, possibly corresponding to a historical earthquake from 1626 AD (Tatevosssian et al., 2011). Dating results from Trench 2 indicate a similar age of the faulting in the Iešjávri Fault System. In this updated map from Olesen et al. (2021) and Olsen et al. (2022) ^{14}C-dating results in cal. yr BP (mean age; 2σ uncertainty interval) are listed for seven of the trenching sites (1, 2, 3, 5, 7, 8 & 9). The faulting events are generally younger than the dating results.

Geological and geophysical setting

The 90-km-long SFC dips at an angle of 30–75° to the SE and can be traced on reflection seismic data to a depth of c. 500 m (Olesen et al., 2021), and may well extend downward. The SFC was up to last year grouped into three fault systems (Olesen et al., 2021; Olsen et al., 2022), but new field-data and dates have led to a subdivision of the complex into two major systems separated by a c. 12 km long gap without any apparent faulting (Fig. 2). Therefore, the fault segments were most likely formed during two or more separate earthquakes (Wesnousky, 2008). Because of the large rupture lengths (≥14 km), the fault systems extend most likely to a depth of several kilometres (Olesen et al., 2021). The SFC (Fig. 2) is located within the regional c. 4–8 km wide Mierojávri-Sværholt Shear Zone (MSSZ) in the Precambrian of Finnmark, northern Norway (Olesen et al., 1992a; Olesen & Sandstad, 1993; Siedlecka & Roberts, 1996; Bingen et al., 2015; Henderson et al., 2015; Mrope et al., in press). The seismic profiling (Olesen et al., 2021) shows that the regional MSSZ dips at an angle of c. 43° to the southeast and can be traced down to a depth of c. 3 km on the reflection seismic profile (Olesen et al., 2021).

The dip of the reverse postglacial faults as observed in trenches is 50–55° implying a maximum reverse displacement of approximately 9 m, which together with the 42 km length of the Máze Fault System indicates an associated earthquake with a moment magnitude of 6.4–8.0 (Olesen et al., 2021), which is here adjusted to 6.9 if a single rupture event is considered and just one magnitude model used (Wells & Coppersmith, 1994; Table 1).

The central part of the SFC in the Máze area occurs at the north-western boundary of the MSSZ while the southern and northern parts are in the middle of the fault zone. MSSZ (Fig. 2) constitutes the north-western margin of the Jergul Gneiss Complex (Siedlecka & Roberts, 1996). Mylonites along the MSSZ can be observed in a roadcut immediately to the north of Nieidagorži along the main road between Masi and Kautokeino. Olesen et al. (1992a) interpreted a dextral displacement along the MSSZ and related the contractional Biggevárri duplex to the Palaeoproterozoic deformation. Structural mapping by Henderson et al. (2015) later verified this interpretation. Diabases several hundred metres thick and albite diabases intruded along the MSSZ 2,220 ± 7 Ma ago (Bingen et al., 2015). These dykes and sills are deformed due to later movements along the fault zone (Solli, 1988; Olesen et al., 1992a). The deformation is mostly related to the Svecofennian orogeny (c. 1 700–1 900 Ma).

The SFC is sub-parallel to the Caledonian front located 25 km farther to the northwest (Figs. 1 & 2) and similar sub-parallel setting is also observed for the postglacial Pärvie Fault (Lundqvist & Lagerbäck, 1976) located in northern Sweden (Fig. 1). The SFC seems to die out along the Guovžiljohka valley in the northeast, but may possibly extend farther to the northeast, although now concealed underneath large boulder fields. The regional MSSZ continues, however, farther to the northeast and the Late Ediacaran to Cambrian Dividal Group is downfaulted by 100 m to the southeast along the MSSZ (Townsend et al., 1989; Siedlecka et al., 2011). The above-lying Caledonian nappes that were thrusted during the Silurian are not offset. The altitude of the lowermost sole thrust varies, however, significantly along the MSSZ farther to the north towards Lakselv. The MSSZ must consequently represent a long-lived fault-zone (Olesen et al., 1992a, 2021). Precambrian shear zones were reactivated in the Čáskejas area during the Timanian orogeny in the latest Ediacaran to early Cambrian (Andresen et al., 2014; Bjørlykke et al., 2022).

The last regional glacial movements across Finnmarksvidda (for location, see framed area in Fig. 1, which cover a central and northern part of Finnmarksvidda) during the last glaciation were mainly from S to N, with some small deviations locally, as indicated by e.g., the direction of drumlins and other streamlined glacial landforms, like flutes (Olsen et al., 1996). This is similar or close to the direction of some of the fault segments and may thus occasionally cause problems to separate glacial lineaments from fault lines in some areas.

The SFC and the Pärvie, Laisvall and Sorsele Faults in Sweden coincide with a physiographic border (Fig. 1). The mountainous area to the west of the Caledonian front has a higher elevation than the area to the east-southeast. The continental ice sheet was consequently thicker in the eastern area. This would involve more depression during the glacial period and consequently a greater contribution to the subsequent postglacial stress regime. The differential loading of ice across a pre-stressed fault line might consequently be sufficient to cause a reactivation of the faults and weakness zones (Olesen, 1988; Muir Wood, 1989; Olesen et al., 2021). This process cannot, however, explain the formation of the other postglacial faults in northern Fennoscandia.

The SFC crosscuts tills and glaciofluvial deposits (including an esker) on Finnmarksvidda (Olesen, 1988; Olesen et al., 1992b). A total of 70 landslide scarps (Fig. 2), some or all of them possibly earthquake induced, are documented within 20 km from the fault scarp (Sletten et al., 2000; Olesen et al., 2021; Olsen et al., 2022). More than 60 % of these landslides occur south of Máze.

The Stuoragurra faulting has produced distinct deformation and fracturing of the host rock. Percussion and core drilling in the Fitnajohka area revealed a dip of c. 40° to the SE at a shallow depth of c. 100 m (Olesen et al., 1992a, b, 2013; Roberts et al., 1997). The postglacial fault consists of few cm thick zones of clay minerals (fault gouge), within a 1.5 m thick interval of fractured quartzite. The clay zones contain kaolinite, vermiculite and smectite (Åm, 1994) and most likely represent a weathered fault gouge. Several 2–3 m thick zones of lithified breccia occur within a 25 m wide interval and reveal that the postglacial faults were formed within an old zone of faulting and weakness partly coinciding with the margins of deformed Paleoproterozoic albite diabases.

Magnetic modelling of the albite diabase in the vicinity of the drill holes shows a dip of c. 40° to the SE (Olesen et al., 1992a), consistent with the results from the drilling. Seismic refraction surveys and resistivity profiling (Olesen et al., 1992a) show both low seismic P-Wave velocity (c. 3800 m/s) and resistivity (c. 900 Ωm) and indicate a high degree of fracturing.

Trenching across the Fitnajohka fault in the Máze Fault System was first performed in 1998, in a location that did not reveal buried organic materials suitable for radiocarbon dating (Dehls et al., 2000). The till above the fault was folded forming a blind thrust (Dehls et al., 2000). Drilling and geophysical data revealed that the fault has a high groundwater yield (Olesen et al., 1992a, 2004), and Dehls et al. (2000) showed that an unconsolidated fault breccia saturated with high-pressure groundwater was injected more than 15 m into the till during the main rupture event at Fitnajohka.

Bungum & Lindholm (1997) recorded many earthquakes along the SFC. Focal mechanism solutions for five earthquakes recorded along or close to the SFC indicated that the maximum principal compressive stress, S_{Hmax}, is oriented on average NW–SE, i.e., approximately perpendicular to the strike of the SFC. The individual focal mechanisms were located at shallow depths southeast of the SFC surface expression. The reverse/oblique nodal planes were oriented so that one plane could be associated with the fault strike for all events; however, σ_H varied from N–S to E–W (averaging to NW–SE).

Olesen et al. (2021) estimated the earthquake moment magnitudes of the Fitnajohka, Máze and Iešjávri Fault Systems within the SFC from fault offset and length utilising formulas by Wells & Coppersmith (1994) and Moss & Ross (2011), provided that just one major rupture event was associated with each fault system. The moment magnitudes varied considerably applying the two different methods, from 6.4 to 8.0 on Richter's scale. The estimates using the Moss &

Ross (2011) equation for reverse faults give the highest magnitudes. Olesen et al. (2021) concluded that the magnitudes of the three earthquakes associated with the formation of the then described three fault systems were in the order of 7. Additional field data and ^{14}C dates in 2022 have led to a revision of the SFC with a merge of the Fitnajohka and Máze Fault Systems into one system, the Máze (revised) Fault System, of 42 km length, and with just one major associated earthquake (Table 1; Máze 2). The Iešjávri Fault System is kept unchanged.

A total of c. 80 earthquakes were registered along the postglacial faults between 1991 and 2019 (Olesen et al., 2021; Fig. 2). The maximum moment magnitude is 4.0 and, due to the proximity of sensitive seismic stations, the catalogue is likely complete down to around magnitude 1.5. The focal depths vary between 5 and 32 km. Most events are located with a lateral and vertical uncertainty of 4 km or less. On the assumption of a c. 43° dip of the SFC and the Mierojávri-Sværholt Shear Zone most of the earthquakes occur at a distance less than 10 km from these structures (Olesen et al., 2021).

Methods

Trenching and radiocarbon dating

New trenching and accompanying data collection were performed at Máze in 2018–2022, at Stuoragurra NE of Máze in 2020, north of Máze in 2021, and at Fitnajohka in 2019–2022 (all in the Máze Fault System), and in the Iešjávri Fault System at Guovžiljohka in 2019 and at Juovssajávrrit and Borgagurra in 2023. We have used trenching through the sediment overburden transverse to the Stuoragurra Fault scarps as our main method to reveal sediment structures affected by the fault event(s) (e.g., Dehls et al., 2000). Various sized trenches, up to 28 m length, were excavated using 8 – 12-ton machine excavators. Sampling of sediments and buried organics has been performed with the intention of revealing the vegetation history based on the content of pollen (*study not completed due to lack of funding*) and macro plant remains, in addition to identifying terrestrial plant macrofossils suitable for radiocarbon dating. The sediment samples were wet-sieved, before single plant fragments were hand-picked and attempted identified down to species level (Olsen et al., 2022). The suitable samples were subsequently dried at 60°C overnight, weighed and sent for radiocarbon dating at the Poznan radiocarbon laboratory, Poland and at a Beta Analytic laboratory in England. The reported ages were calibrated into calendar years before present (cal. yr BP) with the OXCAL v.4.4 software (Bronk Ramsey, 2009) using the IntCal20 dataset (Reimer et al., 2020).

Plant macrofossil content

Samples from the trenching at Máze were analysed for their macro plant remains content (Table 2), with the aim of increasing our knowledge about the Holocene history of the subarctic vegetation in Finnmark, particularly in the area close to Máze. Plant macrofossil analyses together with palynological studies provide an opportunity to infer and date palaeo-environmental and hydrological changes in the area. Detailed palaeoecological data, age-depth models, and a detailed reconstruction of the environmental conditions around the SFC are beyond the scope of this study and therefore not fulfilled here. However, the results from the plant macrofossil analysis, which is relevant as general information of availability of ^{14}C-dating materials at Máze, are briefly described by Olsen et al. (2022).

	Age,	Sample	Type of sediment -
Depth m	cal yr BP, range 2 σ	number	structure and colour
0.3	668-728	1-19	Modern peat, partly disturbed in lower part, dark grey to black
0.5	315-490	2-19	Deformed laminated lacustrine silt -sand with thin organic horizon, light grey to yellowish brown.
0.7	456-631	3-19	Deformed laminated lacustrine silt -sand with thin organic horizon, light grey to yellowish brown.
0.8	550-658	4-19	Deformed laminated lacustrine silt -sand with thin organic horizon, light grey to yellowish brown.
0.98	751-925	5-19	Deformed laminated lacustrine silt -sand with thin organic horizon, light grey to yellowish brown.
1.0	2350-2695	6-19	Deformed laminated lacustrine silt -sand with thin horizon including lumps of peat, light grey to yellowish brown.
1.07	6275-6394	7-19	Buried peat with small pebbles and boulders, between peat and sand.
1.3	6314-6505	4B-18	Buried peat, partly disturbed, greyish brown to black.
1.5	8429-8753	3-18	Deformed till with lenses of sand with organic bearing material, peat remains, grey to bluish grey

Table 2. Sample depths, ages and descriptions of sediments revealed during trenching in 2018-2019 across the Stuoragurra Fault Complex at Máze, Finnmark, Northern Norway (See location in Fig. 3, Trench 7). After Olsen et al., 2022.

Results and interpretation

Trenching and radiocarbon dating

Máze (Masi)

The aim of trenching was to locate buried peat and gyttja that existed prior to the faulting event, perform radiocarbon dating of samples from the buried organic material, and thus

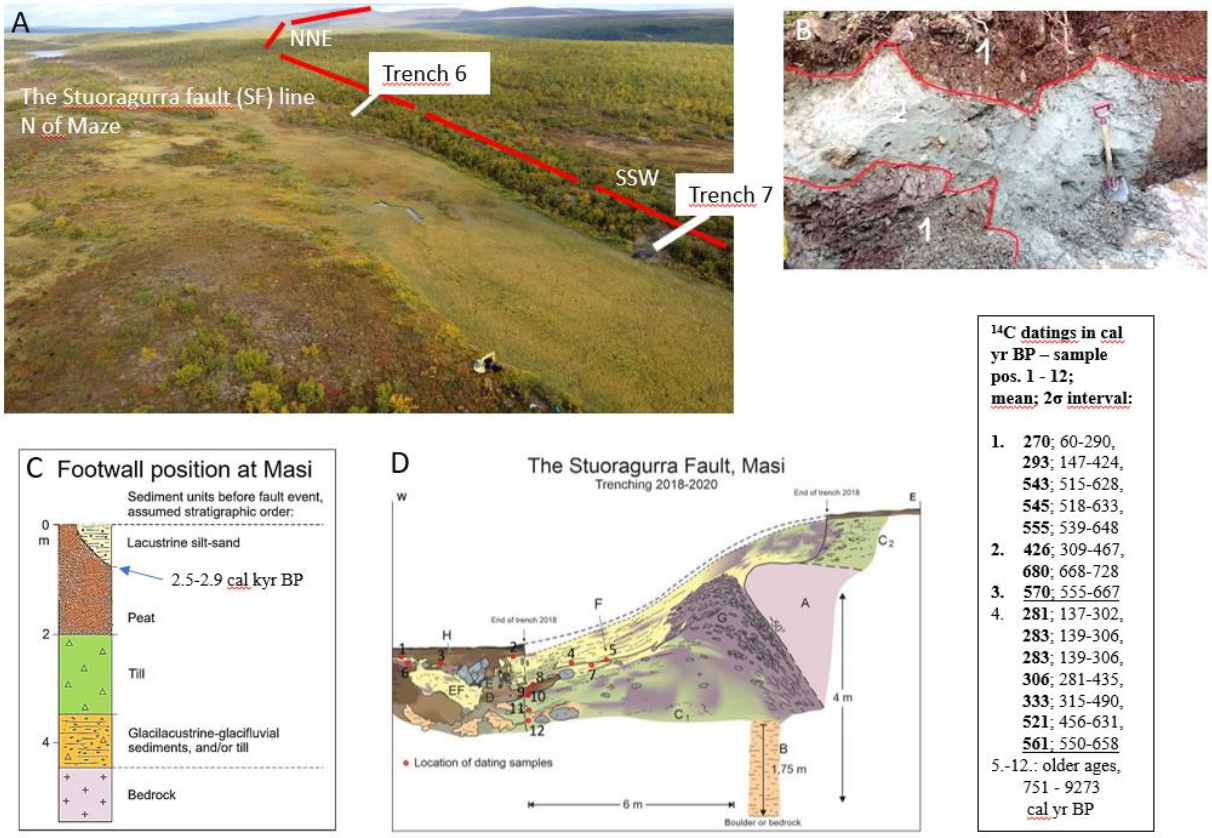

Fig. 4. A: Drone picture of the peatbog along the NNNE trending SF escarpment (stippled line) NW of Máze, with location of Trenches 6 and 7 (see also Fig. 3) shown with white lines. The machine excavator at the western side of the peatbog, c. 40 m W of Trench 7, is representing scale of the picture and position of undeformed 1.8 m thick peat there. Stuoragurra can be seen as a depression in the sky horizon above the "Trench 6" label. B: Deformed sediments (2) on the footwall of the fault, with lenses and overlying wedge of reddish-brown fault breccia (1) in the side wall of the trench transverse to the fault scarp (Trench 6). C: Inferred sedimentary stratigraphy of overburden on the footwall before the last major fault event happened at Máze. D: Outline of the trench (Trench 7 in Figs. 3 and 10) across the Máze Fault System (within the postglacial Stuoragurra Fault Complex) c. 1.5 km to the north of Máze (Figs. 2 & 3). The orientation of the section is normal to the fault. *Enlarged sketch of the section is shown in Figure 7.* The nose of the up-thrown block of bedrock (unit A) is buried by deformed basal till (C_1 and C_2) with deformed lacustrine sand (with thin gyttja layers) (E and F) and modern peat (H), undeformed in the uppermost part, on top. Unit B represents glaciolacustrine or glaciofluvial sediments (silt and fine-grained sand). Unit D is buried and deformed peat, and unit G is wedges of fault breccia (diamicton with angular rock fragments) injected into the sediment overburden during the fault event. Deformed parts of the base layer of the modern peat (H), as well as organic material, mainly plant remains, from the deformed and buried gyttja and peat (from units C_1, D, E and F) are sampled for ^{14}C dating. Positions and numbers of dating samples are shown in the profile. Results to the right are also given in Table 3. Total Holocene peat thickness, c. 0.5-1 m west of the profile shown in D, is recorded to be c. 2.6 m (shown in Fig. 7). Modified from Olsen et al. (2022).

would provide a maximum age estimate for the event. The trenching at Máze revealed deformed sediments, gyttja and peat layers (Figs. 3, 4A, D & 5), which we believe were buried and

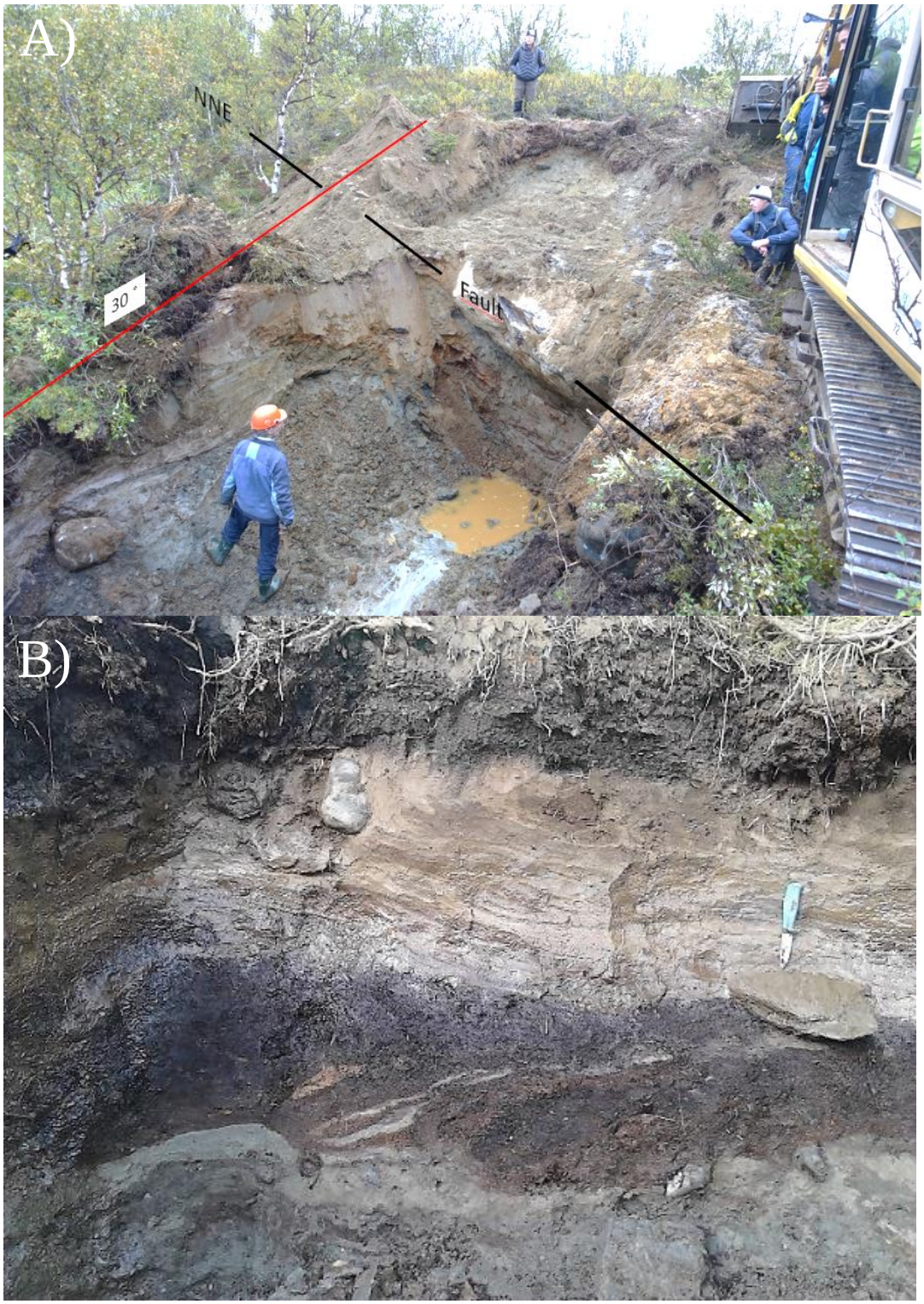

Fig 5. A: Trenching transverse to fault scarp associated with the Masi Fault System in the Stuoragurra Fault Complex, just north of Másí (7 in Fig. 3). Up thrown part of bedrock from the reverse fault is exposed in the central part of the photograph. The hanging-wall or fault plane is dipping c. 50˚ to the right (ESE). Fault breccia, visible in the central part of the photograph, is in contact with the bedrock hanging wall. The fault breccia is produced, pushed, and injected during the fault event into the sediment overburden, with deformation and burial of sediments and organics as a result. B: Partly deformed surficial peat overlying deformed layered lacustrine sand, buried peat and till and glaciofluvial sediments in the 2018-trenching at Másí (7 in Fig.3).

deformed during the main fault event. Radiocarbon dates of macro plant remains from the buried organics and from deformed parts of the base of the topmost 15–30 cm of the surficial peat, indicate that the main young faulting event seem to have occurred after c. 430 cal. yr BP (N=15)(Table 3), which is a mean of fifteen dates, eight of these from deformed organic bearing lacustrine sand, sample positions between 2 and 4 (Fig. 4D), and the other seven of these from the deformed base in the surficial peat directly over deformed sand lenses, sample positions 1, 2 and 3 in Fig. 4D and age ranges based on 2σ standard deviation precision given in Table 3 and Fig. 3. The sand wedges and lenses from the deformed sediments are injected into the existing surficial peat during the main fault event (Figs. 4D & 6).

An attempt to illustrate how we think the overall stratigraphy could have been in the loose material overburden on the footwall side before the faulting event (or events) occurred, is presented in a simplified stratigraphic log (Fig. 4C).

Deposition of the laminated lacustrine sediment overlying the buried peat at Máze (E and F in Fig. 4D; and originally partly overlying and partly adjacent to peat in Fig. 4C) requires a damming by a few dm and up to c. 2 m, i.e. (Olsen et al., 2022), before the major fault event occurred. The damming event may have resulted from sediment collapse and blocking of the outlet, induced by earthquake, with or without an accompanying reverse fault. The bedrock is not exposed in the damming area, so there is no direct visible indicator of an earlier fault event represented there.

Multiple discontinuous wedges of unconsolidated, normal fault breccia injected in the overburden were observed during trenching in 2020 (e.g., Fig. 4B; and Olsen et al., 2022), and some of these may have their origin from a small older reverse faulting event. However, we have not been able to separate these structures clearly from the total deformation pattern.

The damming event is likely to have happened around 2500 - 3000 years before present, which corresponds with the youngest age obtained from the top of the buried peat, and approximately the oldest age obtained from gyttja in the deformed overlying lacustrine sediments as well (Fig. 4D, sample location 6). The sample location 7 in the lacustrine sand represents a re-deposited lump of peat eroded from the buried peat, which is consequently considered to be much older than the lacustrine sediments. We have recorded the total peat thickness to be 1.8-2.75 m in the undisturbed peat some 40 m west of the SFC, just across the mire adjacent to this fault at Máze, Trench 7 (Fig.7). The base of the peat at 1.8 m depth here at the western flank of the mire is dated to c. 8 cal. kyr BP (kyr = thousand years). The peat is supposed to be deeper in the middle

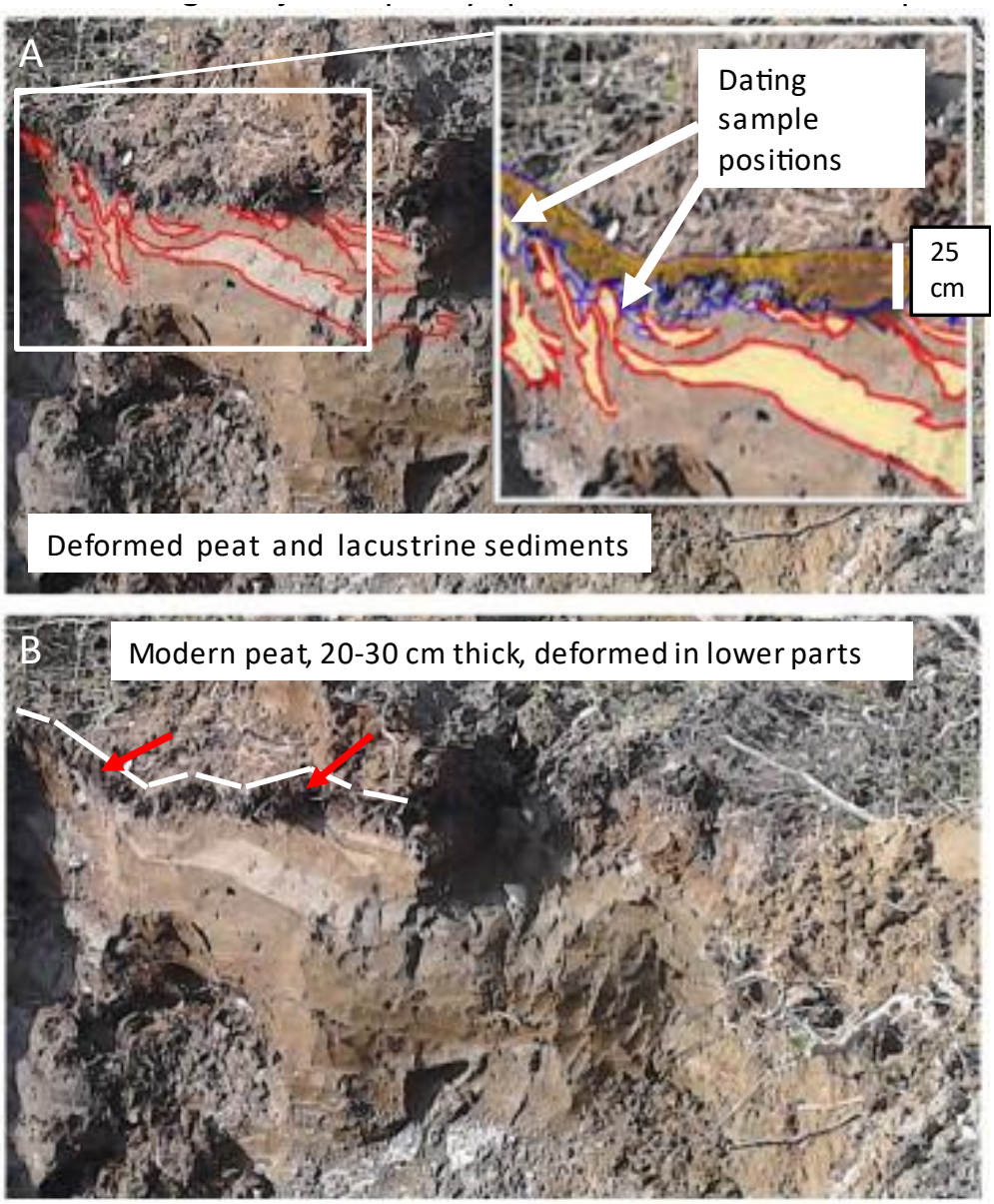

Fig. 6. A, B: sand wedges injected during fault event partly upwards into the modern peat. Positions of dating samples are indicated 15-20 cm from surface of modern peat.

of the mire and started most likely to accumulate there shortly after deglaciation some 11.0 kyr ago. The oldest radiocarbon date from the deformed and buried sediments of c. 9.1 cal. kyr BP (Table 3) in the eastern flank of the mire, where the peat thickness reaches at least 2.6 m close to (c. 1 m outside) Trench 7 (Figs. 4D & 7), supports this hypothesis. This means that the uppermost 15-20 cm of the peat represents c. 6-8% of the total recorded peat thickness, and it represents most likely much less than 660-880 years (c. 6-8%) of the total peat accumulation period (postglacial time), due to compaction of the peat with depth and less organic production, less peat accumulation, during the earlier parts.

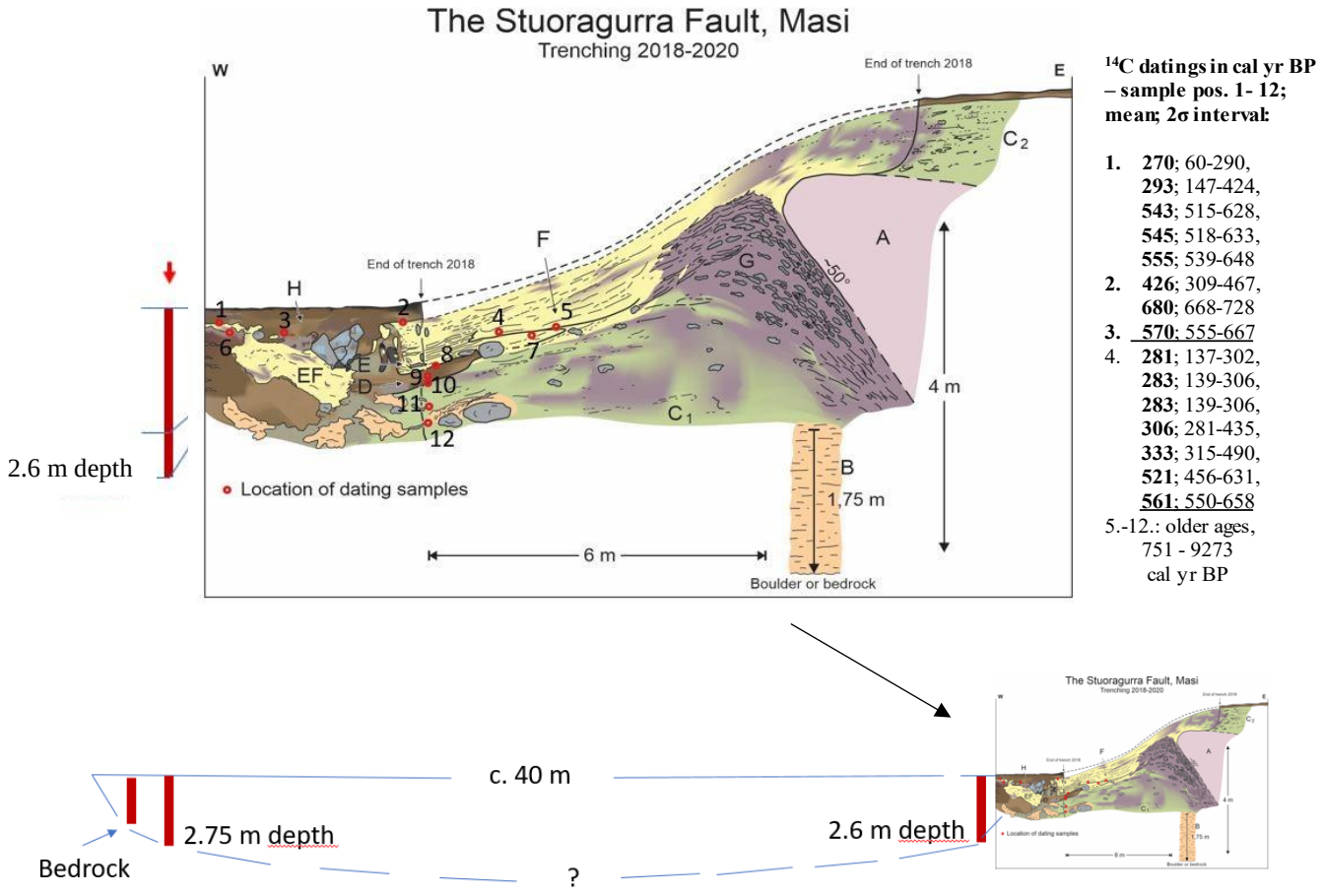

Fig. 7. W-E trending transect across the peatbog adjacent to Trench 7, Máze. *The sediment units are described in the caption to Figure 4.* The total thickness of the Holocene peat is 2.6 m just outside (west of) the trench. Peat accumulation after faulting is less than 15-20 cm, or c. 6-8% of total postglacial peat thickness.

Fitnajohka

Trenching across a SFC fault in the Fitnajohka area was initially carried out in 1998 (Fig. 8; and Dehls et al., 2000), without any finds of buried organics available for ^{14}C-dating. However, deformation structures and clast injections in the sedimentary overburden (Fig. 8C) gave important information of the effect of the faulting there. Folding and push structures in the thick overburden indicated just one dominant faulting event, and injections of thin wedges of unconsolidated fault breccia, reaching at least 12-15 m away from the slip zone under the hanging-wall block of the bedrock. The latter is in odd to other places we have trenched across faults along the SFC, where the overburden is thin and the hanging-wall block of the bedrock

No.	Position in Fig. 4	Field ref.	Lab. ref.	14C-yrs BP ± 1σ	Cal. yrs BP, mean	Cal. yrs BP, 2σ ranges	Yrs AD, 2σ ranges	Comments
	Recent peat, slightly deformed, c. 15-30 cm depth just above deformed lavcustrine sediments and buried peat							
1	1	MASI-3-2022		170 ± 30	c. 270	95.4%: 0-290	95.4%: 1660-1950	
2	1	MASI-2-2022		240 ± 30	c. 293	89:4%: 147-424	89.4%: 1526-1803	
3	2	MASI, STUOR 1-2	Poz-114130	325 ± 30	c. 426	95.4%: 309-467	95:4%: 1553-1711	Macro-plant remains, unspecified
4	1	MASI3-240820-1	Poz-128923	545 ± 30	c. 543	95:4%: 515-628	95.4%: 1392-1505	Leaves and stick, unspecified
5	1	MASI3-240820-2	Poz-129481	555 ± 30	c. 545	95.4%: 518-633	95.4%: 1367-1502	Sticks, unspecified
6	1	MASI-3-2022		590 ± 30	c. 555	95.4%: 539-648	95.4%: 1302-1411	
7	3	MASI1-240820-2	Poz-129478	645 ± 30	c. 570	95.4%: 555-667	95.4%: 1353-1465	Bark, unspecified
8	3' (2)	MASI, Stuor 1-1	Poz-114129	765 ± 30	c. 680	95.4%: 668-728	95.4%: 1292-1354	Sticks and bark, unspecified
	Mean age of 8 samples from c. 15-30 cm dept			479 ± 30	**c. 485**	414 - 561	1431 - 1580	Fault deformation younger than this age
	Upper part of deformed lacustrine sediments							
9	between 2 & 4	MASI2-030919	Beta-543856	190 ± 30	c. 281	78.0%: 137-302	78.0%: 1718-1833	Macro-plant remains, unspecified
10	between 2 & 4	MASI6A-300818	Poz-110597	200 ± 30	c. 283	83.0%: 139-306	83.0%: 1714-1881	0.35 mgC; macro-plant remains
11	between 2 & 4	MASI2B-300818	Poz-110598	200 ± 30	c. 283	89.1%: 139-306	89.1%: 1714-1881	0.6 mgC; macro-plant remains
12	between 2 & 4	MASI3-030919	Beta-543857	270 ± 30	c. 306	89.1%: 281-435	89.1%: 1585-1739	Macro-plant remains, unspecified
13	between 2 & 4	MASI2C-300818	Poz-114132	350 ± 30	c. 333	95.4%: 315-490	95.4%: 1530-1703	0.6 mgC; macro-plant remains
14	between 2 & 4	MASI 2-19, 3-19	Poz-129480	490 ± 50	c. 521	95.4%: 456-631	95.4%: 1389-1564	0.09 mgC; Salix bark and Equisetum fragm.
15	4	MASI4-030919	Beta-543858	620 ± 30	c. 561	95.4%: 550-658	95.4%: 1362-1470	Macro-plant remains, unspecified
	Mean age of 7 samples from deformed sed.:			331 ± 30	**c. 367**	288 - 447	1573 - 1724	
	Mean age of 15 samples, nos. 1 to 15 above:				**c. 430**	355 - 508	**1497 - 1648**	
	Lower part of deformed lacustrine sediments and buried peat							
16	5	MASI2-290818	Poz-110596	945 ± 35	c. 838	95.4%: 751-925		0.11 mgC; stick of birch
17	3	MASI1-240820-1	Poz-128921	2415 ± 30	c. 2522	94.5%: 2350-2695		Bark, unspecified; from peat lump
18	6	MASI2-240820-1	Poz-128922	2800 ± 30	c. 2877	95.4%: 2789-2966		Stick and bark, unspecified
19	6	MASI2-240820-2	Poz-129479	2825 ± 30	c. 2927	95.4%: 2850-3004		Bark, unspecified
20	7	Masi6B-300818-1	Poz-137244	4810 ± 50	c. 5531	95.4%: 5459-5604		Spheroidal Carbonaceous Particles (SCPs)
21	7	MASI6B-300818	Poz-106547	5510 ± 35	c. 6334	95.4%: 6275-6394		0.3 mgC; macro-plant remains
22	8	MASI4A-300818	Poz-110561	5660 ± 40	c. 6409	95.4%: 6314-6505		Wood of birch
23	9	MASI4B-300818	Poz-110560	6030 ± 40	c. 6866	95.4%: 6749-6983		Twig, unspecified
24	10	MASI2A-300818	Poz-106545	6150 ± 40	c. 7036	95.4%: 6909-7163		Macro-plant remains, unspecified
25	11	MASI3-290818	Poz-110595	7810 ± 50	c. 8591	95.4%: 8429-8753		Twig of birch
26	12	MASI1A-300818	Poz-110563	8150 ± 50	c. 9135	95.4%: 8997-9273		Twig of birch

Table 3. Radiocarbon (^{14}C) dates from the Máze trenching site (Fig. 3, Trench 7). Most dating samples are unspecified macro plant remains. Potential roots from modern plants, if observed, have been removed prior to selection of material for dating. However, samples between positions 2 and 4 in Fig. 7A are considered to possibly be affected by modern roots, though not observed in the dating samples. Dating no. 5, with field ref. MASI, Stuor 1-1 is from a position slightly under position 2 in Fig. 7A and is correlated to position 3. Dating no. 11 (MASI 2-19, 3-19) is from fragments of identified plants (Salix bark and Equisetum), and it shows similar age as the accompanying dates (c. 400-600 cal. yr BP) from bulk macro unspecified plant remains from close lying samples. Dating no. 14 (MASI 1-240820-1), is from the deformed lower part of the recent peat and is inferred to represent reworked older material injected into the recent peat during the fault event. Its age deviates significantly from the 13 other dates from the basal part of the recent peat and underlying deformed sediments, and it is therefore put below these in the table. Mean ages are calculated as weighted means between maximum and minimum ages in the 2σ uncertainty age range intervals and are in most cases very close to the associated mean ages in the calibration table presented by Reimer et al., 2020. Modified from Olsen et al., 2022.

is exposed in the fault scarp. In these cases, the wedges of unconsolidated fault breccia are thick and mainly pushed out upon the footwall overburden (Fig. 9). However, also in these situations the unconsolidated fault breccia wedges extend several metres from the fault scarp before thinning out.

Further trenching in the Fitnajohka area was done in 2019 and 2020 (Olsen et al., 2022), as well as last year when we, c. 800 m north of the 2018-trenching, found sedimentary deformation structures and buried and deformed peat and organic bearing lacustrine sediments like those recorded at Máze (Figs. 4, 10, 11 & 12). Location of samples taken for ^{14}C-dating is shown in Fig. 12D.

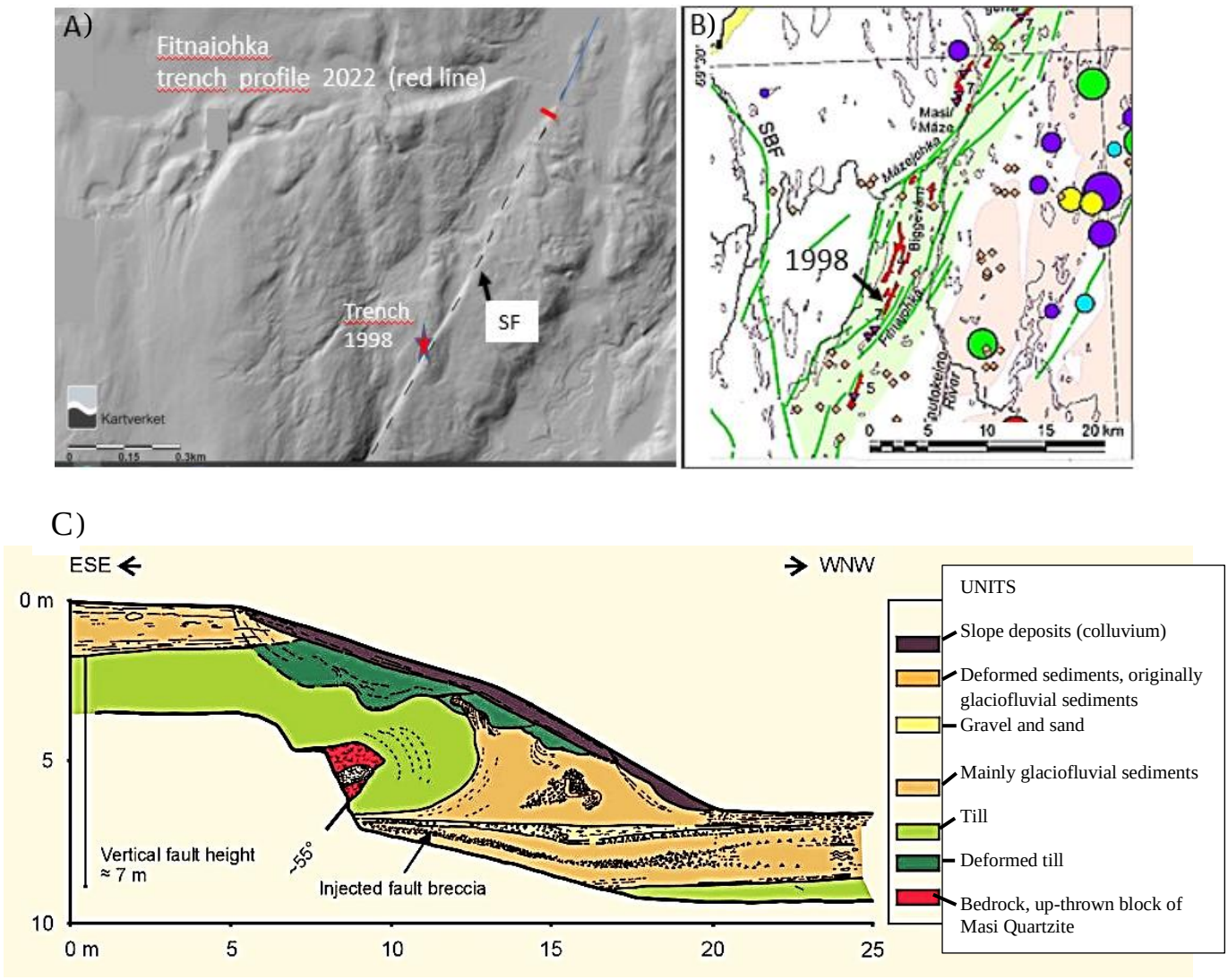

Fig. 8. A, B: Location of trenching from 1998 in the Fitnajohka area (Trench 9, Fig. 3), across the Stuoragurra fault (SF) (stippled line in A) appearing as a distinct lineament in the LiDAR image (A). C: Profile of trench wall with deformed Quaternary sedimentary overburden and nose of the up-thrown hanging wall block (violet) of bedrock. The structures appear as representing one major faulting event, with one major folding of the overburden, and injections of thin wedges of fault breccia, indicated as dotted lines extending from fault plane under the hanging wall and several metres away (westwards) from the fault. The excavation did not reach bedrock of the footwall. Modified from Dehls et al. (2000).

Results from all trenching sites

Trenching with radiocarbon dating of buried or deformed older organic material from Fitnajohka (Figs. 8, 10, 11 & 12), Máze (Figs. 4 – 7; and Table 3), Borgagurra (Fig. 13), Juovssajávrrit (Figs. 14 – 15), and Guovžiljohka (Fig. 16) (Olsen et al, 2022; and Table 4) indicate that the fault events may have happened at almost the same time at the different locations; younger than c. 500 years ago (N= 21) at Máze and Fitnajohka in the Máze Fault System, and possibly less than c. 380 years ago (N= 4) at Juovssajávrrit in the northern part of

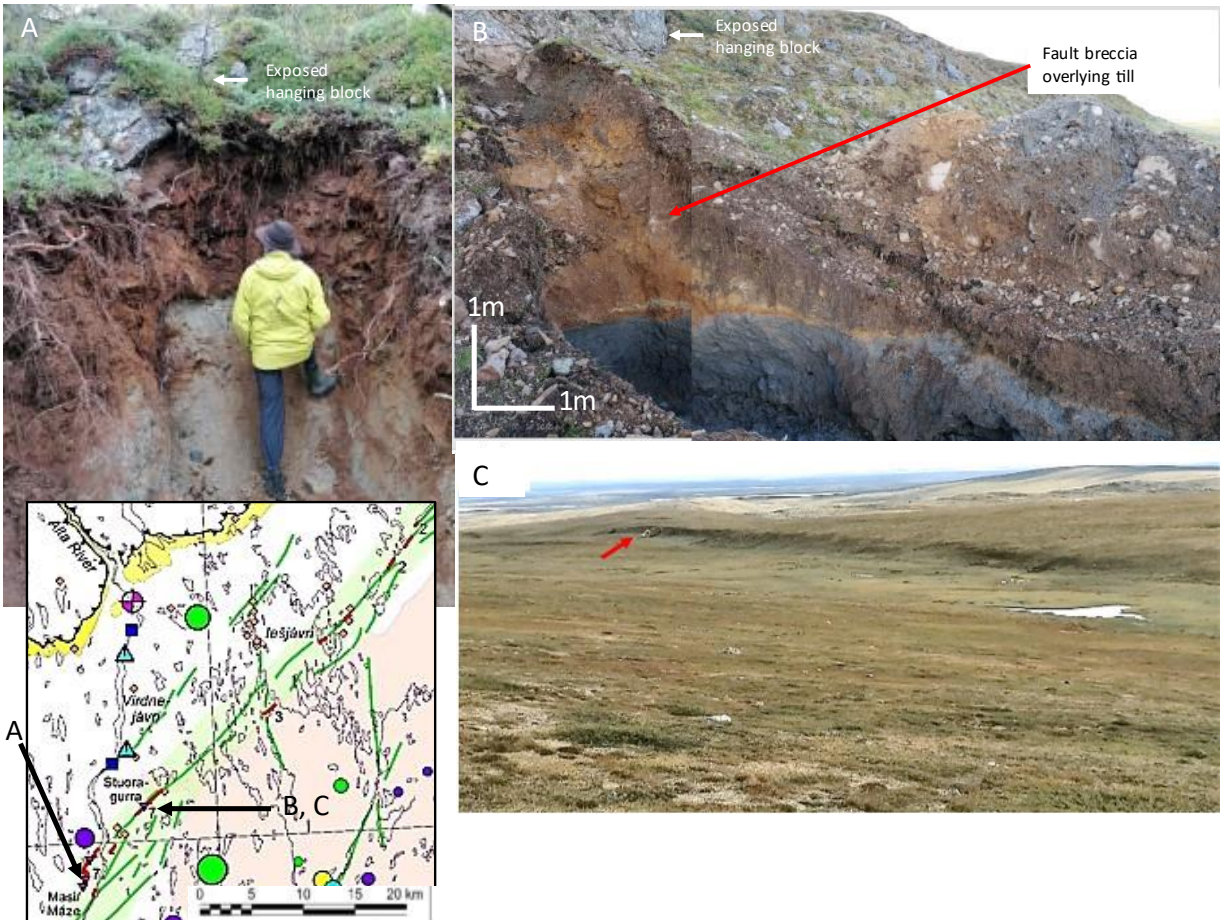

Fig. 9. Examples of thick wedges of fault breccia (brownish colour) in areas with thin Quaternary sedimentary overburden along the fault scarp in the SFC, here at Máze (A) and Stuoragurra (B, C). Locations shown with arrows on the key map (left). Parts of exposed hanging wall block in the fault scarps are indicated to the upper left on the pictures (A & B). C: The NNE-trending (left) fault scarp at Stuoragurra, in the Máze Fault System. An 8-tons machine excavator is located at the trenching site at the foot of the c. 7 m high fault scarp, to the left (red arrow), and is used as scale here.

the Iešjávri Fault System (Figs. 3, 4, 9, 15, 17 & 18) (Table 3: nos. 1-15; Table 4: nos. 37-41 & 53-56). However, the dating results from Borgagurra and Guovžiljohka in the northeast may indicate an older, but still a late postglacial age for the faulting there, i.e., less than 2700-4000 years ago (Table 4: nos. 29 & 59). The interpretation that the fault event is younger than the dated age of the deformed base of the surficial peat at 15–20 cm depth in Trench 7 at Máze (Fig. 6) is based on the observed wedges of sand which are injected to this level horizontally or slightly upward into the existing surficial peat during faulting event (Figs. 4D

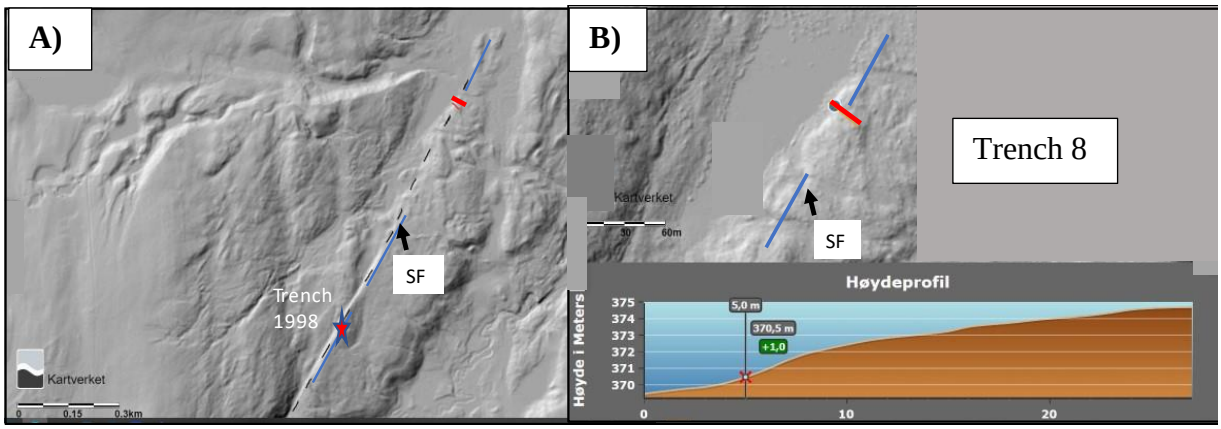

Fig. 10. A: LiDAR image with the Stuoragurra fault (SF) in the Fitnajohka area, indicated with a stippled line. Positions of trenching in 1998 (Trench 9; red asterisk) and 2022 (Trench 8; red line) are shown; B: Position and height profile of Trench 8.

& 6). A similar interpretation is suggested for the stratigraphy at Fitnajohka (Trench 8, Figs. 8 & 10–12) and Borgagurra (Trench 3; Fig. 13). The previous interpretation of the age of the faulting at Trench 5 north of Máze is less straight-forward than the one at Trench 7 at Máze (Fig. 3; Olsen et al., 2022). This is because the dated bark fragments sampled from the top of a few mm thick silt-sand blanket draped upon the unconsolidated fault breccia on the footwall found in Trench 5 are inferred to be re-deposited organics together with the thin silt-sand blanket, just after impact of unconsolidated fault breccia upon the adjacent lake bottom. During impact the lacustrine silt and sand, together with organic remains, would be whirled up in the water and then slowly settled upon the fault breccia outlier when the movement calmed down. This would give a thin blanket of silt-sand with organic remains, including, e.g., fragments of bark on top, just as it was recorded there (Olsen et al., 2022). If not re-deposited, then the age of the bark fragments may indicate an age younger than the fault event there, i.e., about 1.6 cal. kyr BP (Table 4: no. 49). If re-deposited as we suggested earlier (Olsen et al., 2022), then the faulting was younger there. The latter is supported by ^{14}C-dating of a new sample of plant remains from the base of the surficial peat which was disturbed by the push sediments in front of the fault scarp at the same site (633 cal. yr BP; Fig. 3 & Table 4, no. 36). The age of the fault event at Guovžiljohka (Fig. 3; Trench 1) is more straight-forward to suggest since it must be younger than the top of the buried peat there (Olsen et al., 2022).

Data from the trenching of the SF during the 2023 field-season show that the faulting age in the Iešjávri Fault System is also young, like the Máze Fault System, provided that just one postglacial faulting event formed this northeastern system. This happened probably less than 288-432 and more than 329 cal. yr BP based on ^{14}C-dating of macro plant remains in lenses of

organic material in deformed sediments and from the base of the surficial peat or soil on top of the deformed sediments in the fault scarp at Juovssajávrrit (Figs. 15 & 16; Table 4: nos. 53-56). The formation of the Iešjávri Fault System may represent an aftershock of the somewhat older and larger Máze event.

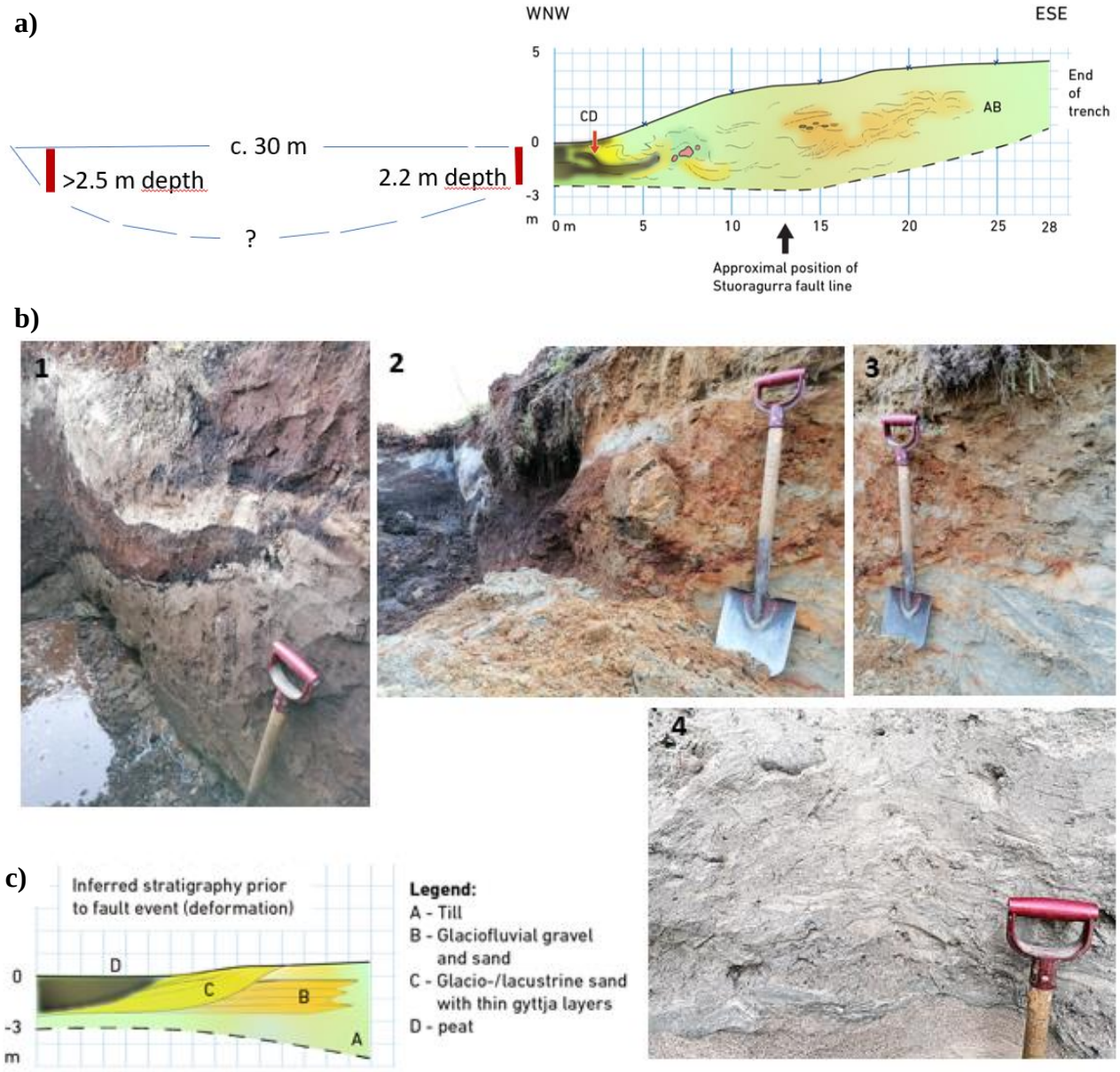

Fig. 11. a: W-E transect across the peatbog adjacent to Trench 8, Fitnajohka. The total thickness of the Holocene peat is 2.2 m just outside (west of) the trench. Peat accumulation after faulting is less than 15-20 cm, or c. 7-9 % of total postglacial peat thickness. To the right, sketch of profile section along Trench 8, Fitnajohka (2022), transverse to the SF, c. 800 m north of Trench 9 (1998), in a zone with thick overburden so that bedrock was not reached during trenching. Units A, B, C and D are as indicated before faulting event in figure c; b: Pictures 1, 2, 3 & 4 show details along the trench from west (1) to east (4), crossing the zone with a folding including a boulder to the left of the shovel in 2 and illustrated in the profile sketch in figure a; c: Inferred sedimentary stratigraphy in the trenching area before the faulting event.

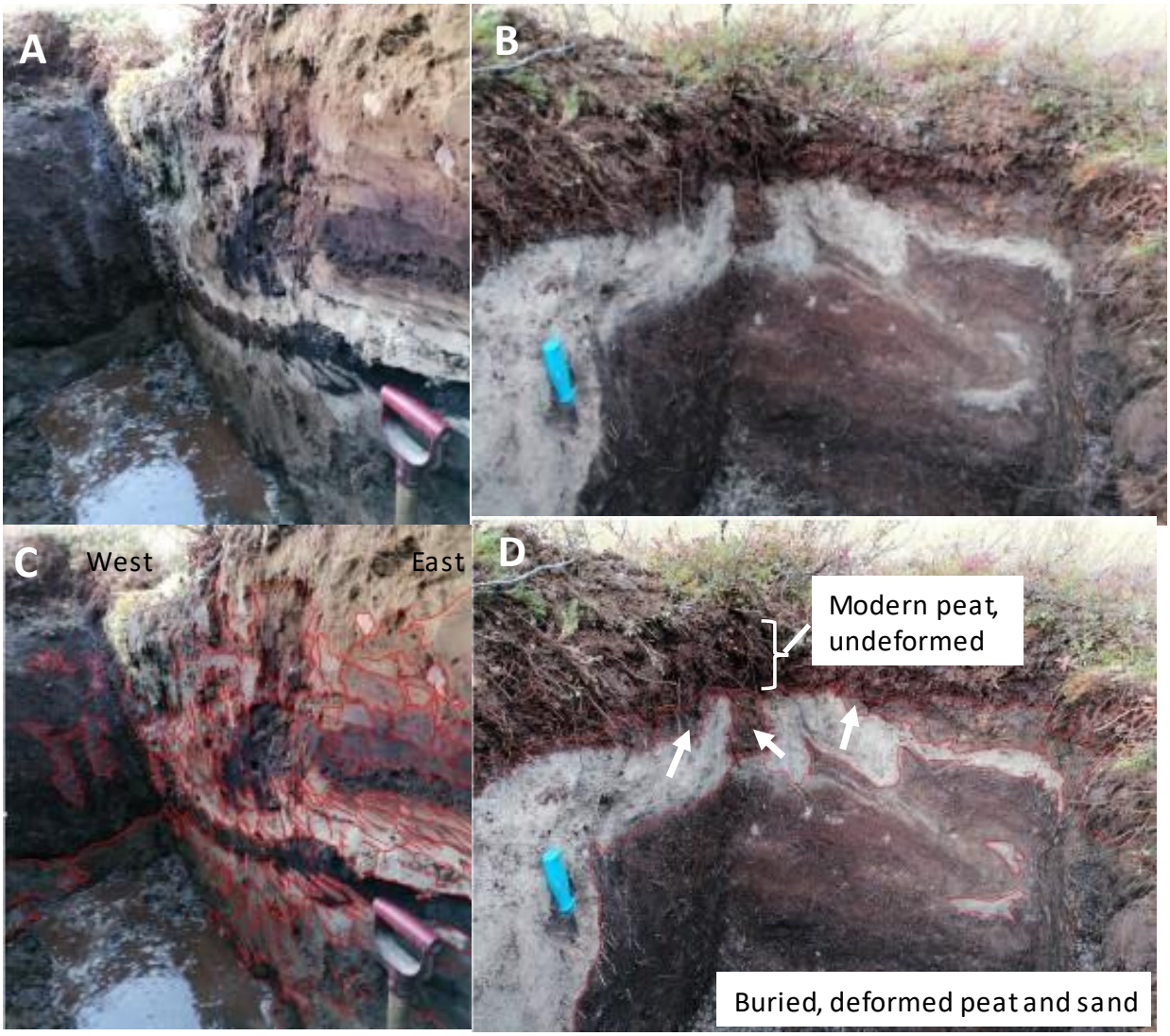

Fig. 12. A, C: Fitnajohka Trench 8, western part of northern trench wall, heading west, away from fault scarp. C: Push structures, shearing and stacking in the overburden, induced by fault deformation movement towards the west. B, D: Western end of Trench 8. Dating sample positions shown by white arrows in D.

Soft sediment deformation and liquefaction

Features like soft sediment deformation structures (SSDSs) occur frequently in the sediment walls of all trenches directed transverse to and crossing the faults in the SFC (e.g., Figs. 6, 11 & 12). Most of these structures have a ductile or plastic movement appearance, with folding, push and squeezing. To get such structures require some degree of water saturation and accompanying liquefaction of the sediments during the deformation (faulting) event. The much less frequently occurring structures with dm to m-high sediment faults or series of smaller faults induced by brittle deformation indicate either dry un-frozen sediment conditions or alternatively frozen ground during faulting within the SFC.

No.	Field ref.	Lab. ref.	14C-yr BP ± 1σ	Cal. yr BP, mean	Cal. yr BP, 2σ ranges	Yrs. AD, 2σ ranges	Comments	Trench nos.
29	Guovz4-300819	Beta-540040	3650 ± 30	3976	95.4%: 3888-4084		Macro plant remains, buried peat	1
30	Guovz3-300819	Beta-543862	5710 ± 30	6490	95.4%: 6410-6617		Macro plant remains, buried peat	1
31	Guovz1-300819-2	Beta-543866	7880 ± 30	8640	95.4%: 8591-8856		Macro plant remains, buried peat	1
32	Guovz2-300819	Beta-543861	8010 ± 30	8990	95.4%: 8773-9007		Macro plant remains, buried peat	1
33	Guovz1-300819-1	Beta-543865	8150 ± 30	9025	95.4%: 9009-9243		Macro plant remains, buried peat	1
34	Masi3-11/9-21	Beta-606448	1660 ± 30	1537	95.4%: 1416-1690		Bark fragments, base top peat	5
35	Masi3-2022	Beta-	111 ± 16	250	95.4%: 0-261	1689-1950	Possible modern, base top peat	5
36	Masi3 4-12/9-22	Poz-163601	625 ± 30	633	95.4%: 548-660	1290-1402	Plant remains, base top peat,def.	5
37	Fitna 4-9/9-22A	Poz-164517	180 ± 30	278	95.4%: 0-293	1657-1950	Plant remains, base top peat,def.	8
38	Fitna 2022-1A	Poz-159578	240 ± 30	293	95.4%: 147-424	1526-1803	Plant remains, base top peat,def.	8
39	Fitna 2022-1B	Beta-	260 ± 30	303	93.8%: 150-434	1516-1800	Plant remains, base top peat,def.	8
40	Fitna 2022-2	Beta-	380 ± 30	474	95.4%: 318-504	1448-1632	Plant remains, base top peat,def.	8
41	Fitna 4-9/9-22B	Poz- 163595	645 ± 30	647	95.4%: 554-668	1282-1396	Plant remains, base top peat,def.	8
42	Fitna3-020919-2	Beta-543864	1120 ± 30	1053	95.4%: 956-1172		Macro plant remains, buried peat	8
43	Fitna3-020919	Beta-543863	1260 ± 30	1243	95.4%: 1086-1282		Macro plant remains, buried peat	8
44	Fitna 2022-3	Beta-	2660 ± 30	2758	95.4%: 2739-2848		Macro plant remains, buried peat	8
45	Fitna 2022-4	Beta-	4110 ± 30	4580	95.4%: 4522-4816		Macro plant remains, buried peat	8
46	Fitna 2022-5	Beta-	4380 ± 30	4559	95.4%: 4860-5042		Macro plant remains, buried peat	8
47	Fitna 2020-1	Poz-129483	5820 ± 40	6650	95.4%: 6529-6734		Macro plant remains, buried peat	8
48	Fitna 2022-6	Beta-	6510 ± 40	7425	95.4%: 7325-7497		Macro plant remains, buried peat	8
49	Masi 1-30/8-21	Poz-145156	1765 ± 30	1628	95.4%: 1571-1718		Undeformed peat, twigs	west of no. 7
50	Masi 2-30/8-21	Poz-145237	4895 ± 35	5600	95.4%: 5583-5716		Undeformed peat, twigs, leafs	west of no. 7
51	Masi 3-30/8-21	Poz-145238	3030 ± 30	3217	95.4%: 3083-3347		Core, peat, twigs, leaf	west of no. 7
52	Masi 4-30/8-21	Poz-145239	6970 ± 40	7790	95.4%: 7693-7925		Core, peat, twigs, leaf	west of no. 7
53	Juovssajavrrit 2A-24/8-23	Beta-675002	280 ± 30	308	95.4%: 288-432	1504-1795	92.4%: 1504-1666 AD. Macro plants	2
54	Juovssajavrrit 2B-24/8-23	Beta-675003	210 ± 30	285	95.4%: 0-306	1642-1950	81.1%: 1642-1808 AD. Macro plants	2
55	Juovssajavrrit 3A-2478-23	Beta-675004	30 ± 30			1694-1917	Macro plants, base top peat	2
56	Juovssajavrrit 3B-24/8-23	Beta-675005	50 ± 30			1694-1918	Macro plants, base top peat	2
57	Borgagurra 1-25/8-23	Beta-675006	118 (0.44 pMC)	Modern			Plant roots, buried peat	3
58	Borgagurra 2-25/8-23	Beta-675007	122 (0.46 pMC)	Modern			Plant roots, buried peat	3
59	Borgagurra 3-25/8-23	Beta-675008	2550 ± 30	2724	95.4%: 2498-2750		Macro plants, deformed peat	3
60	Borgagurra 4-25/8-23	Beta-675009	2840 ± 30	2956	95.4%: 2865-3058		Macro plants, deformed peat	3
61	Borgagurra 1-26/8-23	Beta-675010	3410 ± 30	3641	95.4%: 3568-3819		Macro plants, deformed peat	3
62	Masi SE 10/9-21	Poz-145421	Modern	Modern			Gyttja, young slide, min. age	
63	Masi N 1-11/9-21	Poz-145422	Modern	Modern			Surficial peat, base layer	
64	Masi N 2-11/9-21	Poz-145423	1830 ± 30	1719	95.4%: 1631-1823		Gyttja, young slide, min. age	
65	Rass 2020-4	Poz-128858	Modern	Modern			Surficial peat, base layer	
66	Rass 2020-3	Poz-128857	3020 ± 30	3212	95.4%: 3143-3341		Landslide 2, max. age	
67	Rass 2020-2	Poz-129527	7660 ± 35	8420	95.4%: 8388-8537		Landslide 1, min. age	
68	Rass 2020-1	Poz-129482	8580 ± 50	9540	95.4%: 9481-9676		Landslide 1, min. age	
69	Suolov. S, 1	Beta-	145	Modern	95.4%: 26-261		Landslide, base peat, 15 cm depth	
70	Suolov. S, 2	Beta-	113	Modern	95.4%: 42-251		Landslide, base peat, 10 cm depth	
71	Mathesjavri 1-28/8-23	Beta-675011	111 (0.41 pMC)	Modern		1956-1999	Peat, young landslide, min. age	
72	Mathesjavri 2-28/8-23	Beta-675012	6350 ± 30	7265	95.4%: 7167-7414		Peat, landslide, min. age	
73	Porsangmoen V, 1	Beta-	105	Modern	95.4%: 42-251	1956-2009	Rock avalanche - rock glacier	
74	Porsangmoen V, 2	Beta-	410 ± 30	494	95.4%: 328-518	1432-1622	Rock avalanche - rock glacier	
75	Altadammen 1A-30/8-23	Beta-676313	100 ± 30			1683-1936	Rock fall, macro plant remains	
76	Altadammen 1B-30/8-23	Beta-676314	109 (0.41 pMC)	Modern		1956-2002	Rock fall, macro plantg remains	
77	Altadammen 1B-30/8-23	Beta-676315	2260 ± 30	2324	95.4%: 2155-2344		Rock fall, bulk organic sediment	

Table 4. ^{14}C dates from all localities, except from Trench 4 (Stuoragurra) and trenches 6 & 7 (Máze). All ^{14}C dates from trench 7 (Máze) are shown in Table 3. No dates are available from trenches 4, 6, 9 & 11. Modified from Olsen et al., 2022.

Deformation structures in sediments, including both ductile and brittle deformations, have also been observed in sandy sediments within or close to the SFC zone (Figs. 17, 18 & 19), but not necessarily directly connected to the faulting deformation. However, these structures are considered because of deformation possibly caused by strong earthquake(s) along the SFC, before, during or after the main faulting event.

Fault breccia observed at and in the trenches

Lithified fault breccia and injected wedges of unconsolidated, normal fault breccia characterise the contact zone with the up-thrown bedrock block and the adjacent deformed sediment overburden. This is observed in trenches both at Fitnajohka, Máze and Latnetoaivi

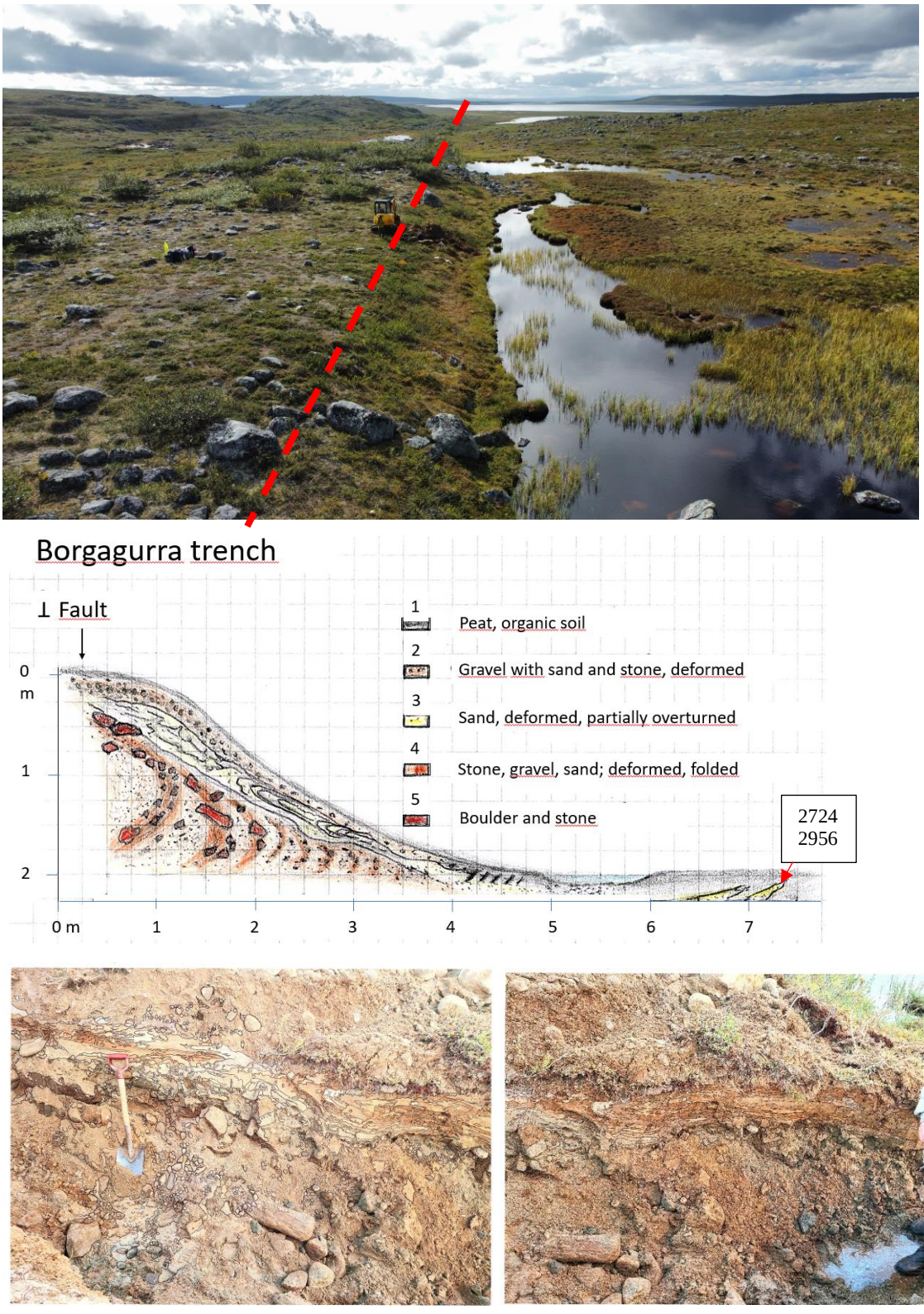

Fig. 13. Upper panel: Trenching across the fault scarp at Borgagurra, 2023 (machine excavator as scale) (Fig. 3: Trench 3). Ages shown in cal. yr BP. Fault direction is indicated by a red broken line. The area is characterised by a thick sediment overburden and the bedrock is not exposed even in the fault scarp. Middel panel: sketch of the trench wall with the main units indicated. All units, except the younger surficial peat-soil, deformed during the faulting event. The sand wedges in the peat to the right some 5 metres from the scarp are assumed pushed into the peat during the faulting. Lower panel: pictures of parts of the trench wall, with structures made visually more distinct by pen linings.

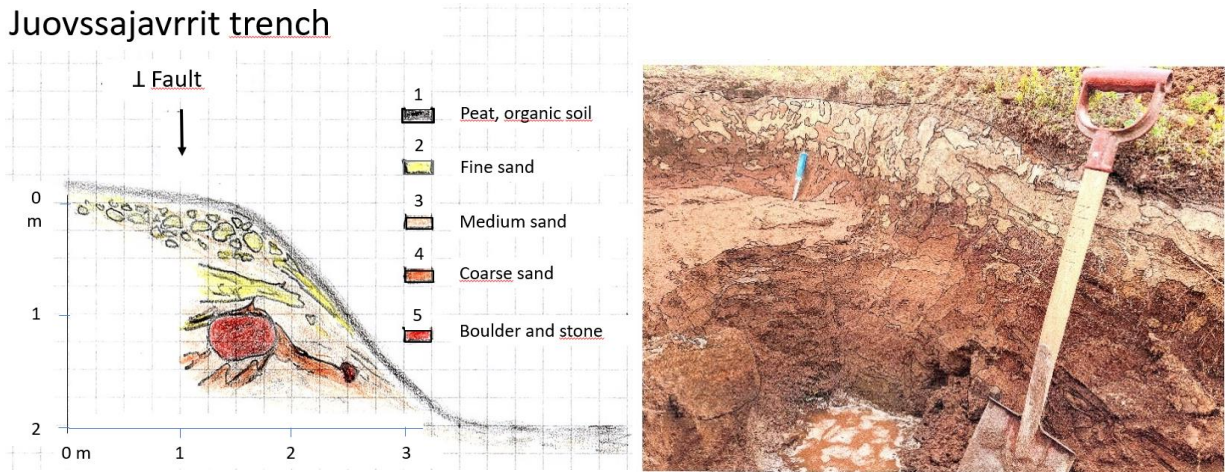

Fig. 14. Upper panel: Trenching by shovel across the SF scarp at Juovssajávrrit, 2023 (Fig. 3: Trench 2). Fault direction indicated by red broken line. The bedrock is not exposed in the fault scarp, and the overburden is generally thick in this area. Lower panel: sketch (left) of the trench wall with the main sediment units indicated. All units are deformed during the faulting event. Picture (right) of parts of the trench wall, included in the cartoon sketch to the left.

(Stuoragurra) in the Máze Fault System (Figs. 3, 4, 5, 8C & 20A; Dehls et al, 2000; Olsen et al., 2022). In addition, angular blocks of local bedrock type have been spread out from the nose of the up-thrown bedrock to at least 15–20 m distance from the fault scarp (Olsen et al., 2022). Fracturing from the exposed hanging wall nose, followed by sliding downward the slope would not alone explain the long distance from the scarp for some of the blocks. Therefore, it is thought that the angular blocks located farthest from the scarp are somehow

Fig. 15. Additional pictures of the trench walls at Juovssajávrrit. Macro plant remains from peat lenses and lumps (2; Table 4, nos. 53-54) in the deformed sediments and in the base of the surficial soil or peat (1; Table 4, nos. 55-56) indicate that the faulting happened here between c. 330 and 430 years ago.

thrown out during the fault event. The wedges of unconsolidated fault breccia consist of mainly angular clasts of local bedrock type, and they are reaching several metres out from the fault scarp (Figs. 8C, 20A & 20B). Lithified fault breccia from the bedrock in the fault area clearly reveals a much older fault history and suggests that the postglacial Stuoragurra Fault Complex represents a reactivated part of a several hundreds of millions of years old tectonically active zone (Fig. 20C; and Olesen et al., 2021).

Plant macrofossils

Details of sample depths, ages and descriptions of sediments revealed during trenching across the SFC at Máze in 2018–2019 are given in Table 2. The results of the macro plant analysis of these samples have been reported by Olsen et al. (2022), and examples of such plant remains, including some of those which have been picked out for ^{14}C dating are shown in Fig. 21.

Some of these samples may have reverse stratigraphic positions, because of possible turnovers from deformation during the fault event(s). Consequently, we have chosen not to make a traditional age-depth model of these data. However, even the preliminary data we have from

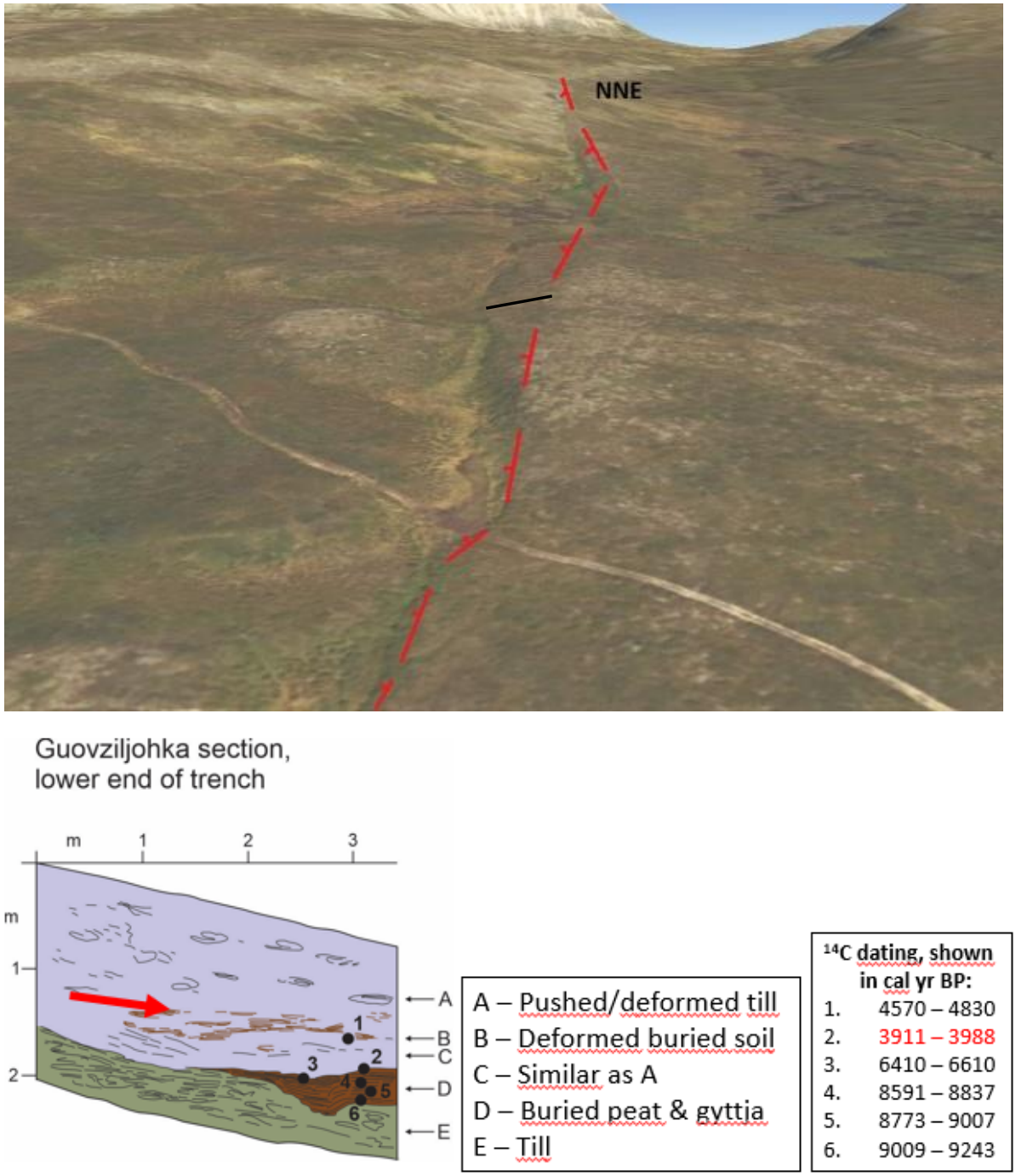

Fig. 16. Upper panel: Trenching indicated by a black line across the fault scarp at Guovžiljohka, 2019 (Fig. 3: Trench 1). The fault trending to the NNE consists here of several fault segments which are in some parts directed at an angle deviating from the next segment along the main fault line, as indicated by the broken red line. Lower panel: Sketch of the lower part of the trench towards the footwall part of the fault, with the main units indicated. ^{14}C dating from the top of the buried peat indicates that the faulting occurred less than 4000 years ago.

macro-plant remains in the disturbed sediments at Máze, indicate quite normal vegetational signatures for sub-arctic vegetation during the different postglacial ages. Typical plant taxa identified in the samples representing early to late Holocene ages between c. 8500 and 400 cal.

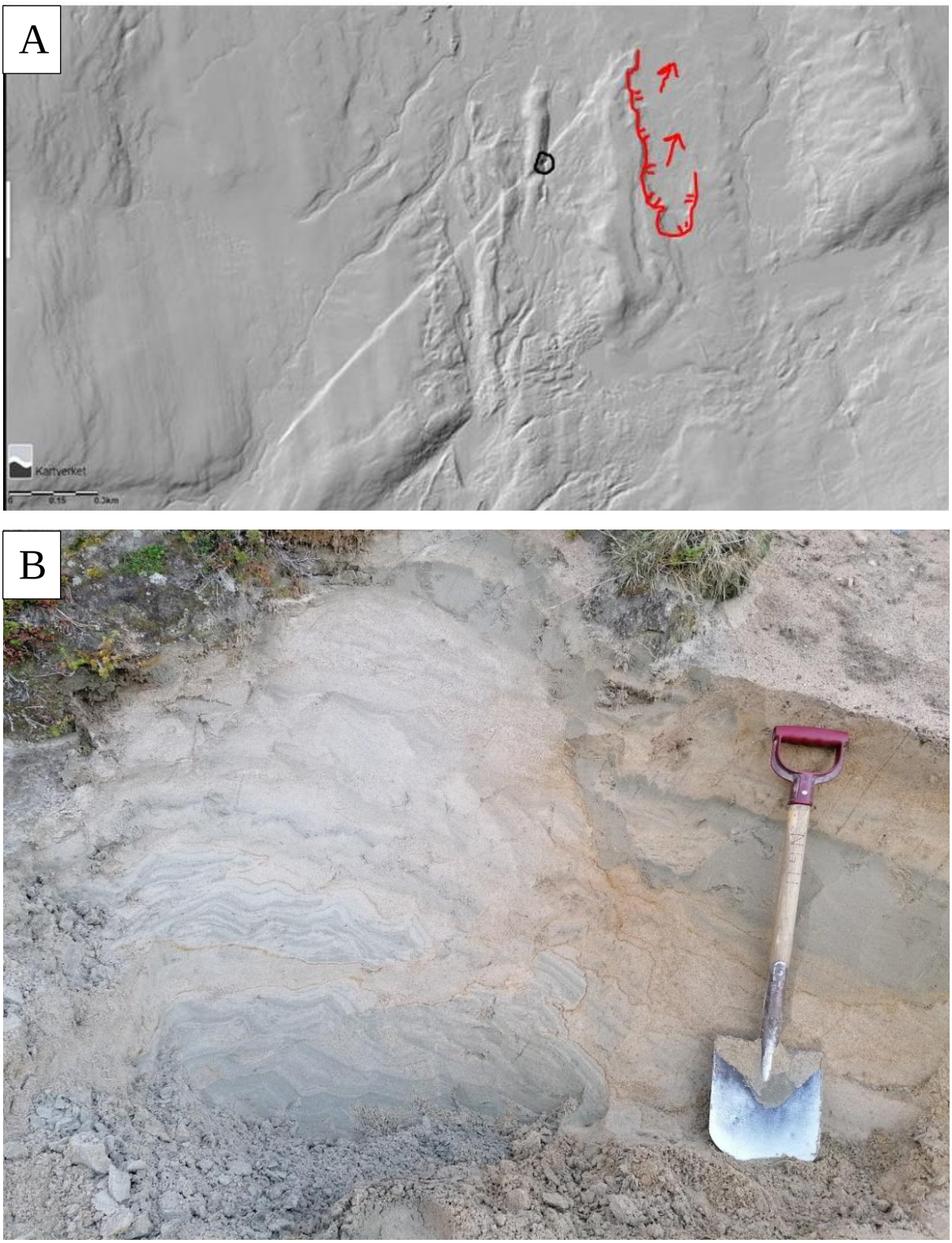

Fig. 17. A, B: Deformed sand in an originally glaciofluvial formation which the fault (NE trending lineament) cuts through at Stuoragurra, NE of Máze. Location indicated with a black contour in the LiDAR image above (A). Slide scar from a slide located close to the fault scarp and directed towards the NE (red arrows) is indicated with red tagged line. B: Enlarged photo of SSDS in the lower part of a several metres high section in the glaciofluvial formation mentioned in A.

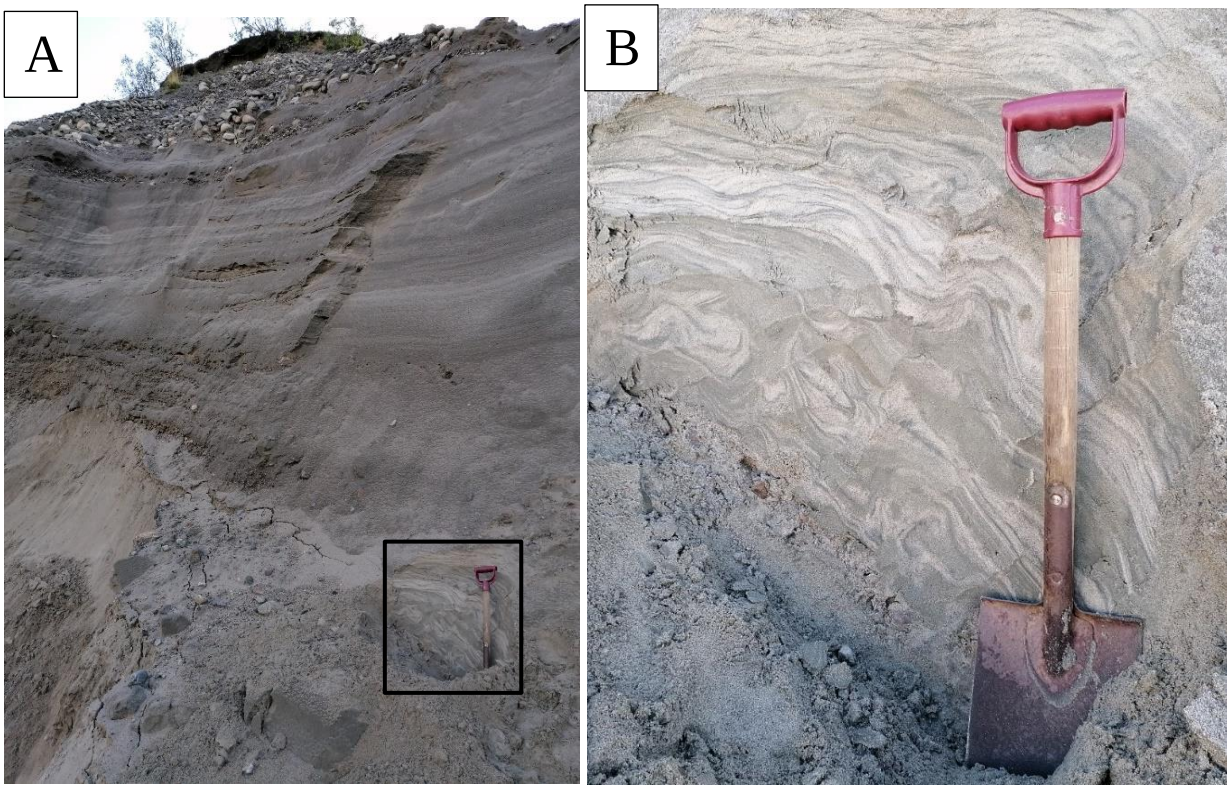

Fig. 18. A (left): Glaciofluvial formation south of and close to the Stuoragurra fault east of Máze, with SSDS in lower parts. Framed part of the section is enlarged in B. B (right): Enlarged part of sand and silt appear with SSDS structures, with folding, slumping and small-scale faulting.

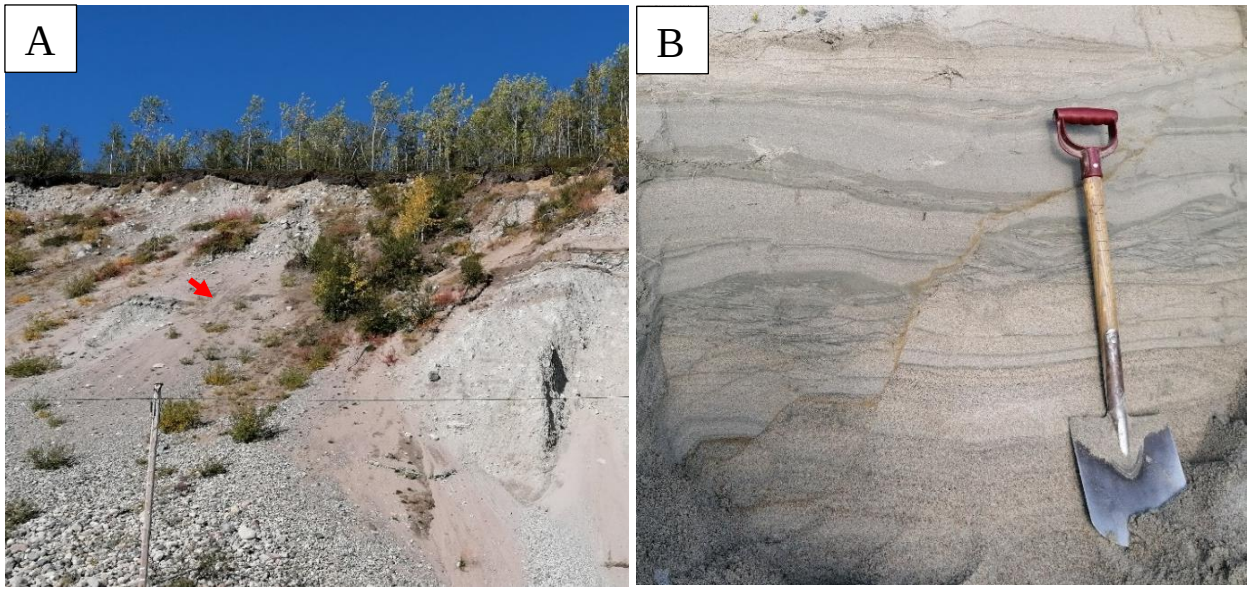

Fig. 19. A (left): Glaciofluvial formation of gravel and sand close to the Stuoragurra fault west of Máze, with deformation structures in sand, including faulting and slumping (B), in the middle of the 15-20 m high sediment wall. Location indicated with red arrow. B (right): Enlargement of section with the mentioned deformations.

yr BP are from trees and shrubs (*Betula pubescens* and *Salix spp.*), dwarf shrubs (*Betula nana, Salix herbacea, Empetrum hermaphroditum*, a.o.), graminoids (*Poaceae, Junceae*), higher spore plants (*Equisetum*), and bryophyta (*Sphagnum ssp.*, a.o.) (Olsen et al., 2022).

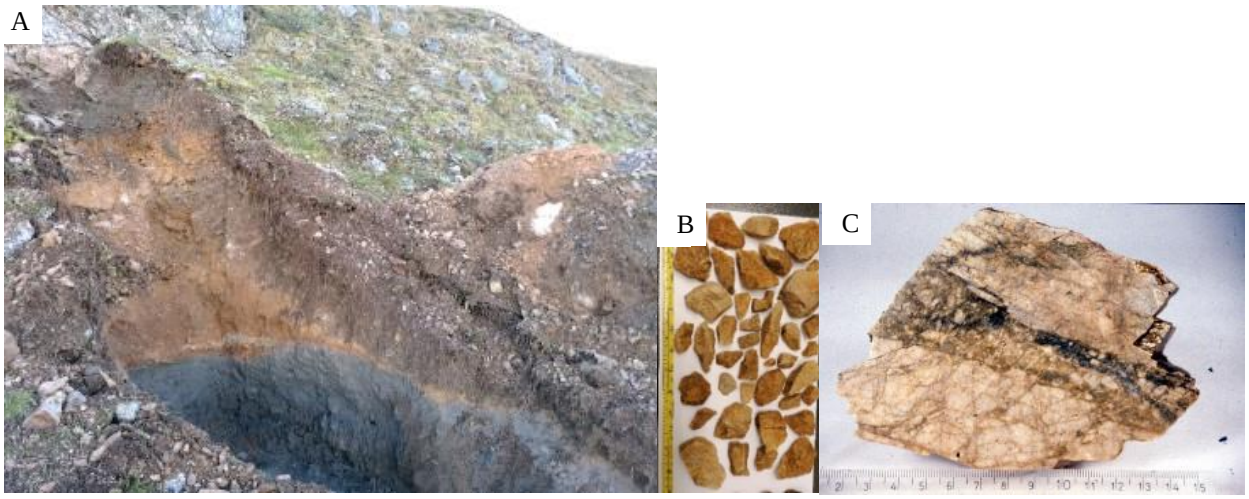

Fig. 20. A: Fault breccia represented as a thick brownish wedge of unconsolidated angular clasts mixed with sandy matrix on the footwall and in the fault scarp at Stuoragurra (Trench 4 in Fig. 3). B: Angular to subangular clasts of parent faulted bedrock from the wedges of fault breccia in figure A. C: Lithified fault breccia from the faulted bedrock in the Ftinajohka area (close to Trench 9, Fig. 3). Similar lithified fault breccia is found at all locations where trenching across the faults in the SFC have reached bedrock (i.e., 7 of 11 trenches), which indicates that the postglacial SFC represents a reactivation of a much older seismically and tectonically active bedrock zone. After Olsen et al. (2022).

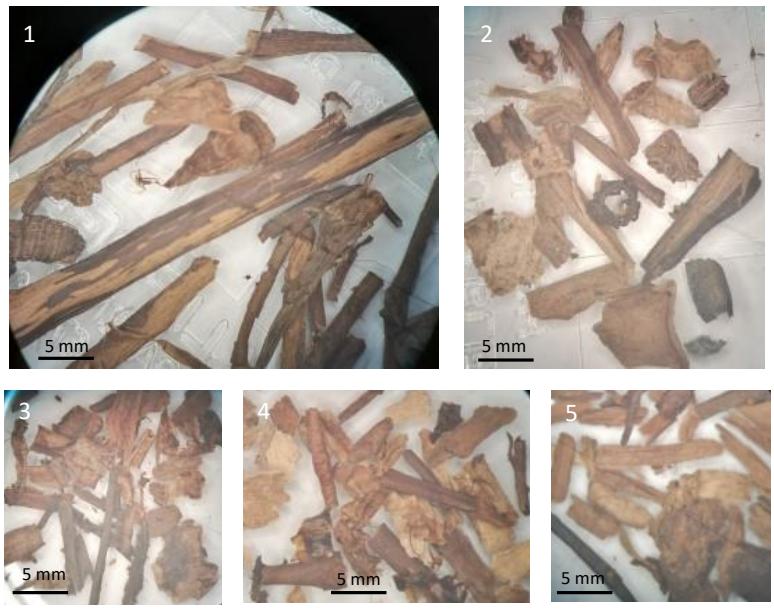

Fig. 21. Examples of macro plant fragments used for ^{14}C-dating from Trench 7, Máze (1, 2), from Trench 8, Fitnajohka (3, 4), and from deformed soil in front of a rock avalanche W of Porsangmoen (5).

Landslides and rock avalanches in the fault area and in adjacent positions

From LiDAR data we have recorded c. 70 landslide scarps in or close to the area of the Stuoragurra Fault Complex (Fig. 3). We have dated landslides in one location in a relatively flat area, west of the mountain Rassegalvarri and close to the Fitnajohka Fault System (location close to Trench 11 in Fig. 3). Two landslides are recorded at this location; (Figs. 3 & 22), one older landslide that seem to have occurred before c. 9.5 cal. kyr BP and formed the main bowl of the slide depression, and one small younger landslide occurring after c. 3.3 cal. kyr BP (Table 4: nos. 65–68). Landslides in four other locations have been studied, one location west and one northwest of Máze, one located 8 km SE of Máze, and one west of Trench 5, N of Máze (Fig. 3 & Olsen et al., 2022). In two of the locations (SE and N of Máze), there have been major landslide episodes during or shortly after deglaciation, with slide morphology integrated fully into the deglaciation landscapes, including, e.g., kettle holes and meltwater channels (Olsen et al., 2022). In the slide location SE of Máze a small landslide occurring within two bigger ones is dated to modern time based on ^{14}C-dating of gyttja in lacustrine silt-sand in a little pond in the slide depression (Fig. 23; Table 4: no. 62).

In the slide location west of Trench 5 a small landslide occurred prior to 1.6 cal. kyr BP (Table 4; no. 64), and there also located within the main bowl of the older bigger one. The latter is however more like a flush channel from the last deglaciation, a hypothesis which is supported by the presence of kettle holes on the top surface adjacent to the flush scar. ^{14}C-dating of gyttja in lacustrine sediments in a pond in the slide depression is also in this case basis for age estimation of the landslide (Olsen et al. 2022).

The two medium sized landslides laterally to a drumlin west of Máze are attempted dated based on ^{14}C-dating of bottom samples of soil in depressions on lower parts of the slides, both yielding modern ages (Fig. 23, and Table 4; nos. 69-70), suggesting a young age of the slides, possible during or just after The Little Ice Age (c. 1500-1920 AD).

A landslide complex laterally to another drumlin, in this case located northwest of Máze (Máhtesjávri), comprising three landslides, a major older one which dominates the main part of the slide complex, and two younger and smaller landslides. The two latter ones have merely moved the backwall of the complex farther into the central part of the drumlin (Fig. 23). ^{14}C-dating of samples from the base of the peat accumulated after each of the two younger sliding events indicate modern age for the youngest slide event and mid Holocene age for the previous one (Table 4; nos. 71-72). The thickness of the peat growing in a depression on the surface of

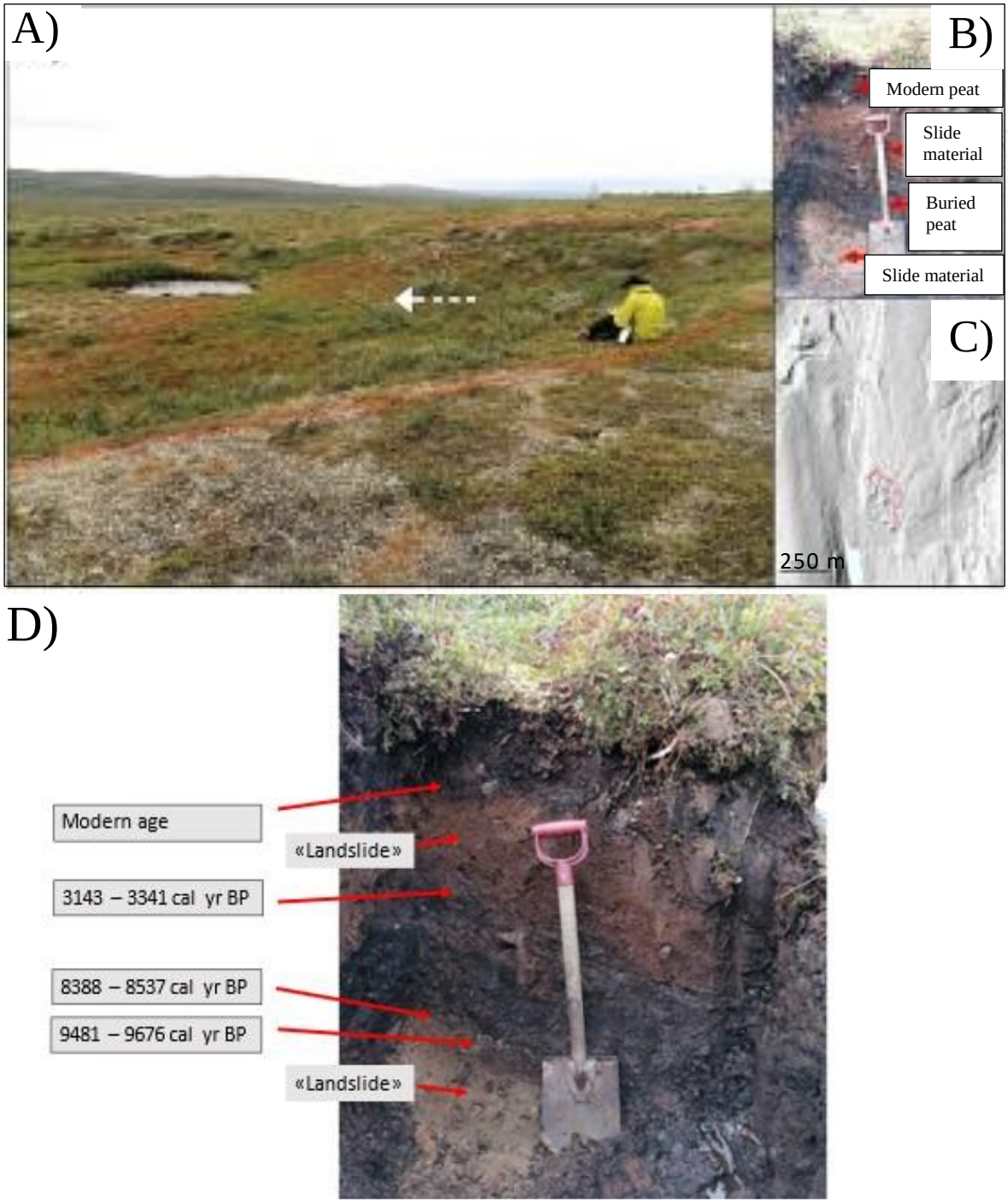

Fig. 22. Landslides in the vicinity of the SFC; A, B, C, D: Two landslides (B, D) recorded and dated in one slide depression (A) 50–250 m from the SF (C; visible as SSW-NNE trending fault lineaments on the LiDAR image) in the southernmost part of the SFC (after Olsen et al., 2022), This locality is also shown in an overview with comparison of four landslide complexes, two laterally to drumlins and two in general flat glacial landscapes in figure 23.

the oldest slide is more than 1 m, which is considerably thicker than the peat growing on the younger slides. Therefore, we assume the oldest slide to be of early Holocene age.

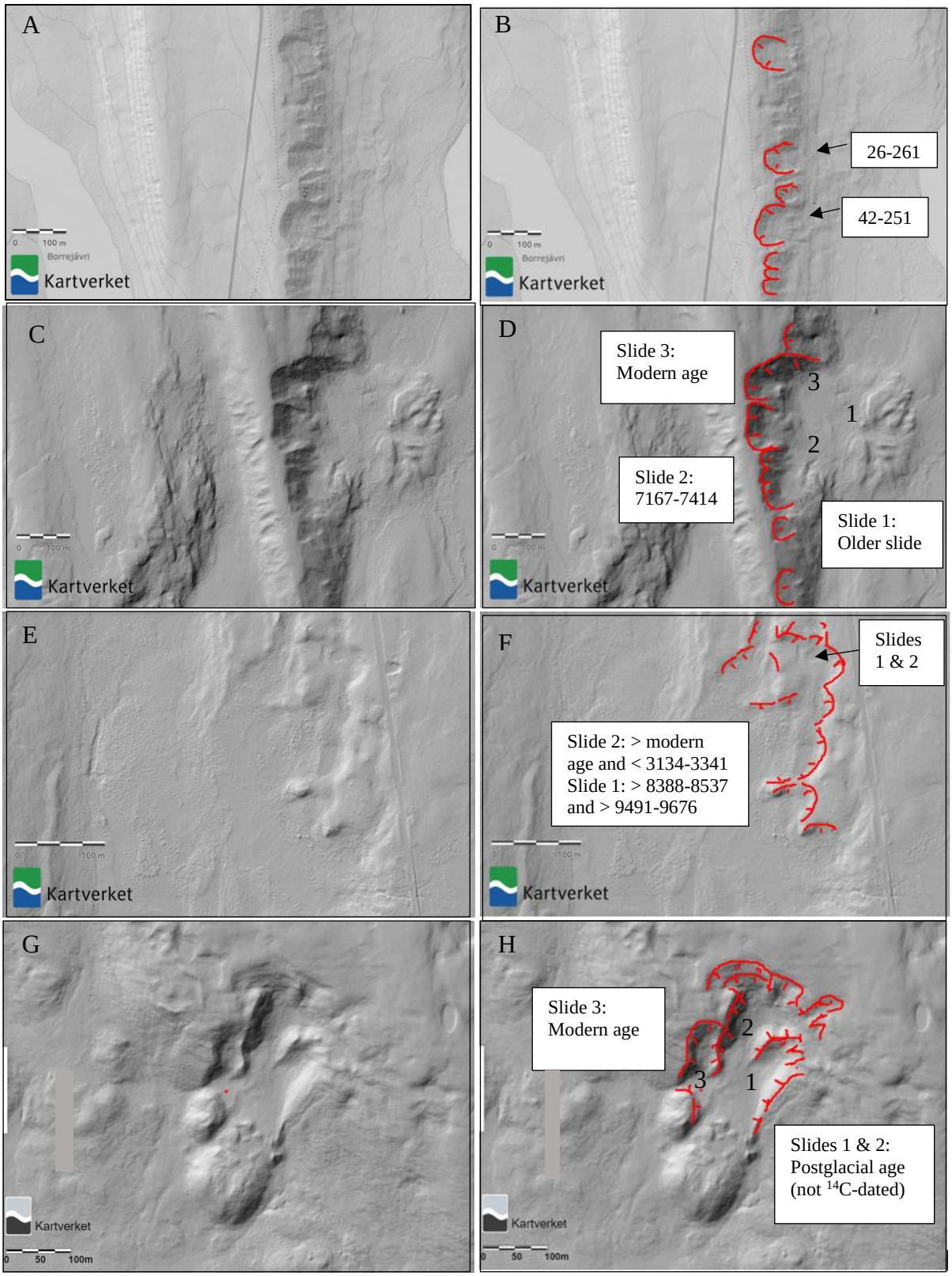

Fig. 23. Landslide complexes in relatively flat terrain just a few hundred metres to a few kms from the SFC, with locations indicated in Fig. 3 as L1, L2, L3 and L4 and squares. The youngest landslide in each complex is from modern time, or just a few hundred years, as indicated by ^{14}C-dating of plant remains from the base of the surficial peat in depressions on the flat lying surface of the slide material at the base of the youngest slide bowl. Older landslides in the complexes are indicated by ^{14}C-dating of plant remains from the base of thicker peat in depressions on the adjacent outer parts (C, D) of the complexes, or in the

top and the base of buried peat underlying slide material (E, F). A, B: Landslide complex L1, west of Máze. C, D: Landslide complex L2, northwest of Maze. E, F: Landslide complex L3, southwest of Máze. G, H: Landslide complex L4, southeast of Máze. Ages given as cal yr BP with 2σ uncertainty and referring to Table 4, nos. 69-70, 71-72, 65-68, and 62.

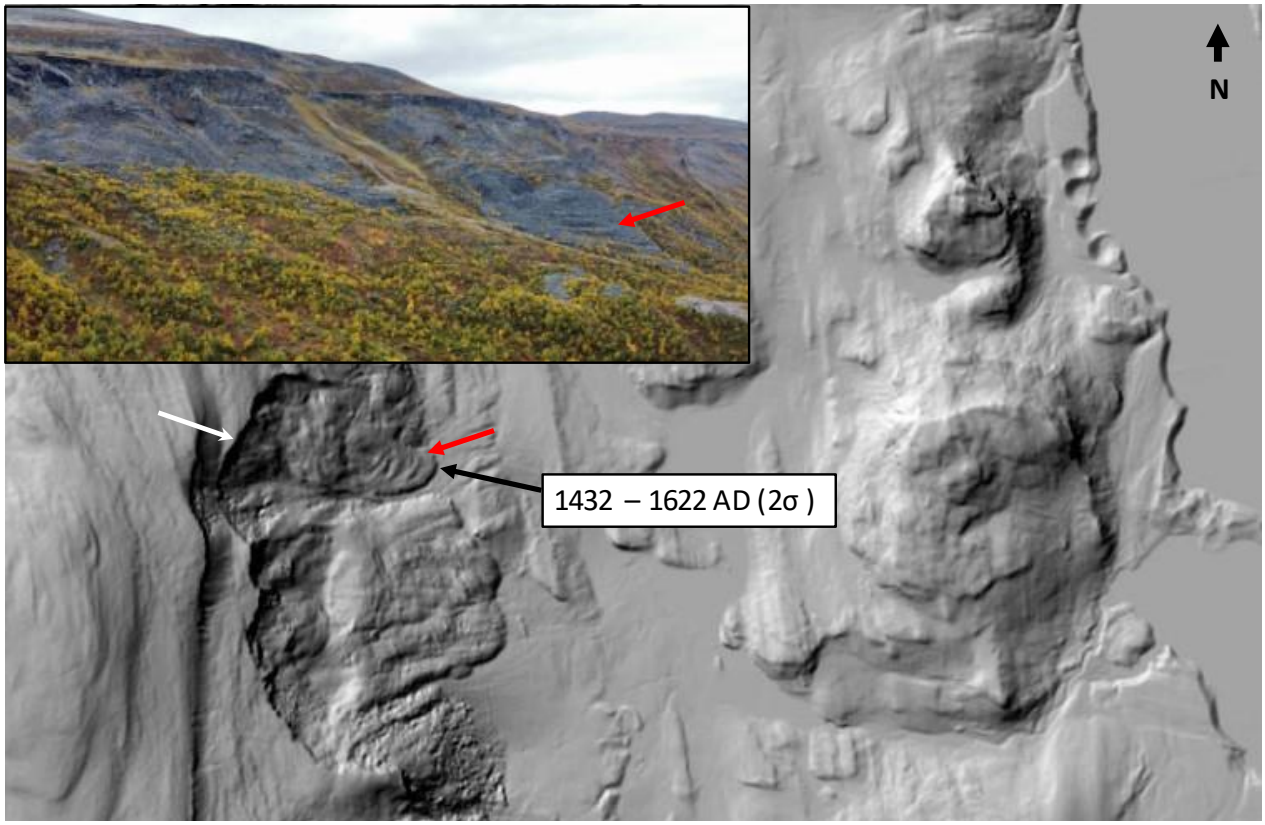

Fig. 24. Rock avalanche west of Lakselv in Finnmark. Lower parts of the avalanche seem to have possibly transformed to a rock-glacier type of formation, with some lobate sliding structures present. Radiocarbon dating of deformed soil is shown, and it indicates deformation during the Little Ice Age (LIA- c. 1500-1920 AD). For location, see upper right corner of Fig. 2. From www.høydedata.no and www.norgeibilder.no

Three medium-sized rock avalanches have been recorded at Ávjovárri 4.5 km to the west of Porsangmoen in the continuation of the fault to the NE, about 10 km from the fault (Figs. 2, 3 & 24). The rock avalanches are assumed to be of a late Holocene age, due to the fresh appearance of the angular edges of the margins of the slip zone. Curvilinear structures in the lower parts indicate that this portion of the rock avalanches or rock fall material (talus), between c. 330 and 190 m a.s.l., has possibly transformed to a rock-glacier type of formation. The location and surface form fit well with other active rock-glaciers in Norway, which in Finnmark often are located above 300-400 m a.s.l. (Hestad, 2021). However, at the northern coast in Finnmark rock-glaciers even reaching almost down to sea-level, and therefore active to the last part of the Litte Ice Age (i.e., LIA; 1500-1920 AD), have been reported by Lilleøren et al. (2022). It is also shown by Linge et

al. (2020) from a study in southern Norway that rock glaciers may form rapidly and be fully active in just a few hundred years. Therefore, rock-glacier formation west of Porsangmoen most likely occurred during LIA. On the other hand, field observations around the rock avalanche – rock-glacier complex west of Porsangmoen indicate that the curvilinear structures there may alternatively be a result of sliding of the avalanche on thick sandy glaciogenic deposits in the steep valley side (Olsen et al., 2022). A ^{14}C-dating of plant macrofossils in deformed soil at the foot of the front-wall of the rock avalanche or rock glacier indicates movement of the associated boulders after c. 494 cal. yr BP (Table 4; no. 74). If this represents a maximum age of the rock avalanche itself or just a subsequent rock glacier formed during the LIA is not known. Two other minor rock avalanches occur along the eastern shore of lake Virdnejávri (Figs. 2 & 3). They are located c. 5 and 13 km northwest of the Máze fault system.

A curvilinear c. 600 m long and c. 100 m wide unstable mountain slope is located c. 120 m above the northwestern shore of the hydropower reservoir behind the Alta Dam (Figs. 3, 25 & 26; Olsen et al., 2022; Olesen & Olsen, 2023). The distance to the Alta Dam and the SFC is 3 and 15 km, respectively. The vertical subsidence seems to be in the order of 20 m along the curvilinear fractures. Open fractures can be observed on arial photographs (www.norgeibilder.no). The back wall consists of gabbro while relatively flat-lying mica schists are out-cropping along the shoreline. The water level of the water reservoir below the unstable rock slope is varying with 45 m during a year and is consequently contributing to further destabilization. The unstable bedrock slope is covering an area of 120 000 m^2. If the unstable area also reaches, e.g., 25 m into the bedrock, then it will include an unstable bedrock volume of c. 3 mill. m^3. The reservoir immediately below the unstable rock slope has a length of c. 600 m, a depth of c. 45 m and a width of c. 110 m. In total, this volume represents c. 1.5 million m^3 of water that most likely will be displaced if up to 3 million m^3 of rock falls into the reservoir. (We have assumed full magazine that will be the situation most of the year.) About half of the water will go northwards in the direction of the Alta Dam, i.e., c. 0.75 million m^3 of water. We recommend that a modelling of this scenario is carried out to predict the water flow in the Alta River. There is also a need to consider at potential damming of the Virdnejávri and Latnetjávri lakes and flooding of the village Máze (Masi) located 30 km to the south (Olesen & Olsen, 2023). The consultancy company NGI is currently carrying out such modelling on behalf of dam owner Statkraft (Oda Alstad Førlie, pers comm., 2023).

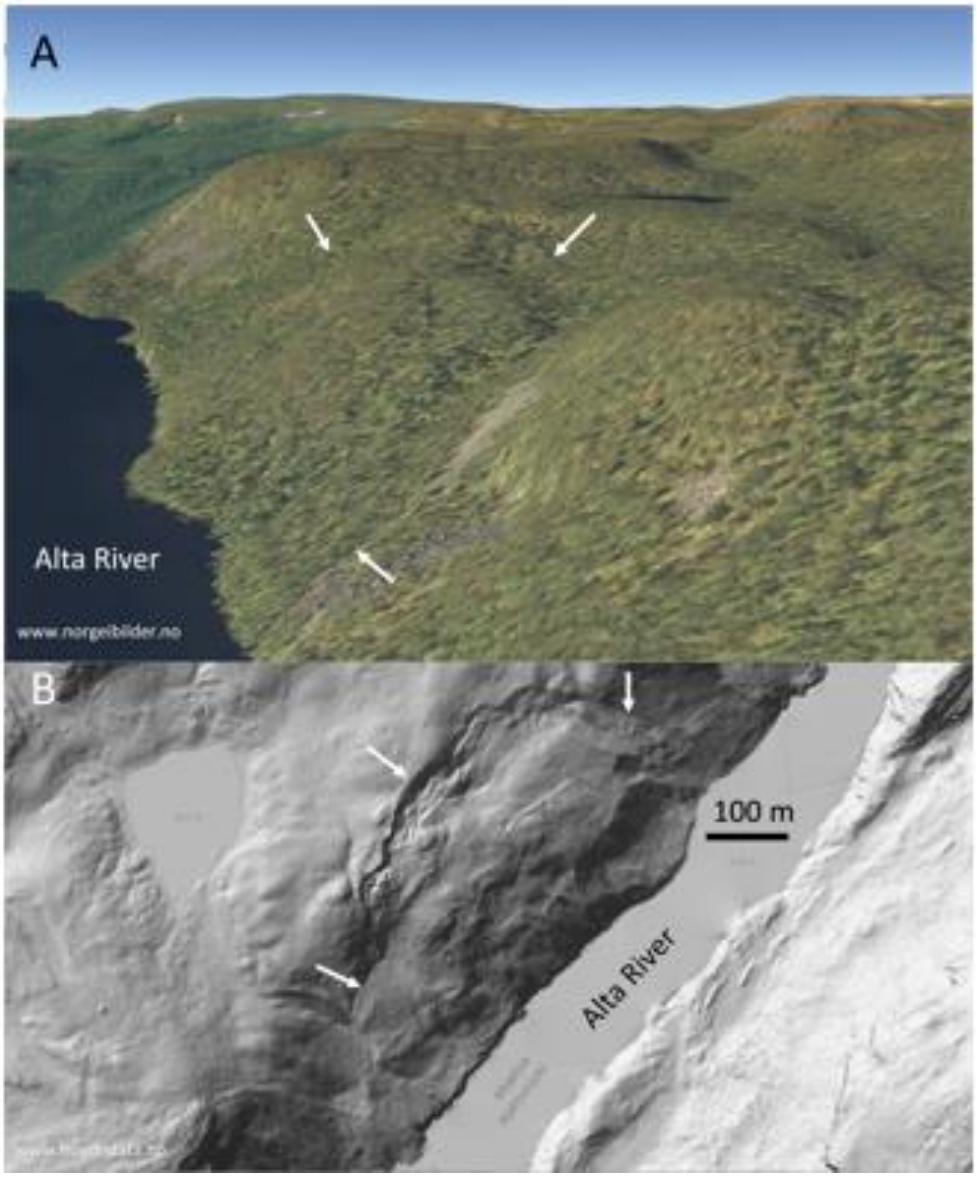

Fig. 25. Unstable bedrock slope covering an area of 120 000 m^2 along the Alta River south of the Alta Hydropower Station Dam, and north of the SFC (Fig. 3). It reaches most likely c. 45 m downwards below the surface of the dammed Alta River. The height of the almost vertical wall at the back of the unstable rock slope is up to 15 m. If the unstable area reaches, e.g., 25 m into the bedrock, then it will include an unstable bedrock volume of c. 3 mill. m^3.

In a direction towards the NE, about 80 km beyond the visible part of the NE trending fault line of the SFC, two rock avalanches of medium size (Terje Solbakk, pers. comm., 2023) are

recorded SW and W of Kunes at the end of Laksefjord (K in Fig. 1). The rock avalanches occur in gentle slopes on rather small mountains (with heights of 180–200 m above the adjacent terrain) and are most likely caused by earthquake shaking. The northernmost of the two rock avalanches is deposited upon a fluvial terrace with top surface 65 m a.s.l., which we assume represents an early postglacial sea level c. 9.5-10 kyr BP. This is based on comparison with the marine limit at

100–120 m a.s.l. from the late-glacial period before YD, and a relatively rapid late glacial to early postglacial shoreline displacement in this area (e.g., Sollid et al., 1973). The age of the rock avalanche west of Kunes is therefore probably early postglacial.

Fig. 26. A (left): Blocks of rock fallen from an up to 20 m high bedrock wall in the uppermost part of the unstable bedrock slope shown in figure 25. B (right): A sample of plant remains was taken from the base (at the knife edge point) of the thickest surficial peat between rock boulders, indicated by red arrow, in front of the adjacent collapsed bedrock backwall shown to the left. A ^{14}C-dating of these plant remains indicate that the bedrock wall collapses probably occurred before 1683 AD (Table 4; no. 75).

Discussion

The Stuoragurra Fault Complex (SFC) consists of at least 29 segments, which are grouped in two fault systems, a northern (Iešjávri) and a southern (Máze) (Fig. 2). The SFC occur within the more than 2 000 million years old Mierojávri-Sværholt Shear Zone (Olesen et al., 1992a), and was earlier sub-divided in three fault systems (Olesen et al., 2021; Olsen et al., 2022). As to date it has not been clear if they formed during one large earthquake or several smaller events. Trenching across one of the southernmost segments in the Fitnajohka area in 1998 (Dehls et al., 2000) reveals one seismic event deforming the lodgement till into a large 5 m high fold above a blind thrust below the hanging wall block. When comparing the SFC with other postglacial faults in northern Fennoscandia (Lagerbäck & Sundh, 2008; Palmu et al., 2015), with emphasis on height and length of scarps and length between scarps, there is evidence for at least two separate seismic events, i.e., the *revised* Máze Fault System (previously named Máze and Fitnajohka Fault Systems) in the central and south-western areas and the Iešjávri Fault System to the northeast. Fault parameters are given in Olesen et al. (2021). Some of the drainage

systems in the area, especially northeast of Iešjávri, are controlled by the same weakness zones in the basement. Streams may have modified the fault escarpments following their formation (Olesen, 1988). The escarpments of the Máze Fault System have maximum scarp heights of 7 m and occur partly in an *en échelon* pattern. The distance between the Máze and the Iešjávri Fault Systems is 12 km. We assume that the Iešjávri Fault System is almost continuous at the floor of the Iešjávri lake since postglacial faults occur on either side of the lake (Fig. 2). Wesnousky (2008) suggests that earthquakes do not typically jump from one segment to another if the distance between the segments is more than 3–5 km. He based this conclusion on a total of 37 historical earthquakes with observed surface ruptures. A spacing of more than 5 km between surface ruptures therefore likely indicates that the earthquakes occurred in separate events. This would support the idea that the two fault systems along the SFC may have ruptured independently. Mattila et al. (2019) arrived at similar conclusions for the postglacial faults in northern Finland.

Radiocarbon dating of buried organics from locations along the Máze Fault System indicate fault events younger than c. 430 cal. yr BP (N=15) at Máze and possibly the same age, or approximately the same age at Fitnajohka (N=6) (Fig. 3; Trenches 7 & 8; Tables 3 & 4, respectively). Sand wedge injections in existing peat leaves no doubt about the faulting age that must be younger than the deformed basal part of the surficial peat, which is deformed below 15-20 cm depth at Máze, Trench 7, as illustrated in Fig. 4D and further described in the text. The total Holocene peat thickness just 1 m west of the western end of Trench 7 is c. 2 .6 m (Fig. 7), which implies that the surficial 15 cm of the peat represents just 6% of the total 11 kyr Holocene peat, i.e., c. 660 years. Considering, e.g., compaction of the peat with depth, and low organic production early and peat accumulation in postglacial time, it seems most likely that the surficial 15-20 cm of the peat represents just a few hundred years of accumulation, and it also implies a very young age of the faulting. The faulting age at Fitnajohka is apparently also younger than c. 430 cal. yr BP, based on ^{14}C-dating of plant macrofossils, and similar stratigraphy and deformation structures there (Figs. 8–13; Trench 8) as found at Máze. These data may therefore well represent the same faulting event both places.

However, there are some data suggesting the occurrence of a smaller postglacial faulting event at Máze before the major one. This is exemplified by the multiple wedges of unconsolidated fault breccia injected into the overburden on the footwall at Trench 6 (Fig. 4B), and the damming event which led to accumulation of lacustrine sediments revealed in Trench 7 may just possibly be associated with a minor reverse fault event. Therefore, we cannot conclude with

the present-day knowledge if all these data represent just one major faulting event, or one major and one or several minor faulting events.

The apparently very young ages achieved from radiocarbon dating of the SFC at Máze (Trench 7) and Fitnajohka (Trench 8) require special attention to the reliability if these dates. It is well known that plant roots may give much too young ages of organic material in peat or minerogenic sediments at depth, this is considered and observed roots are not included in the dating samples. However, very small sticks that might be fragments of plant root systems may have been attached to other plant fragments and not detected during cleaning of samples for dating, and by that may have biased the dating results. This may possibly have affected the dating results from the uppermost part of the deformed lacustrine sediments at Máze. However, we observe that the age results of these dates overlap, or are just slightly younger than, and do not deviate significantly neither from those of close-lying samples, nor from the dates at 15–30 cm depth in the deformed basal parts of the surficial peat. In addition, most dating materials from the deformed lacustrine sediments are bark and twigs (mainly from birch; Fig. 21) which we think are normally good ^{14}C-dating materials and not particularly susceptible for young C-contamination. Considered that the lacustrine sediments were injected and pushed into the surficial peat during the faulting event, the youngest part of the lacustrine sediments should be older than the fault and younger than the deformed basal parts of the overlying surficial peat, at 15–30 cm depth, i.e., just above the lacustrine wedges (Figs. 4D & 6). Based on observations of vertical traces of recent or sub-recent plant roots in the trench walls in the deformed lacustrine sediments we chose earlier to exclude the dating nos. 9-13 from the data used to estimate maximum age of the youngest fault event (Olsen et al., 2022). However, no plant root remnants were observed in these dating samples, and their ^{14}C ages overlap clearly with, and do not deviate significantly from the other dates of the upper part of the deformed sediments. Therefore, we now include all these samples (total number N= 15) to estimate maximum age of the youngest fault event (Figs. 3 & 27). Similar considerations and conclusion have been done for the Fitnajohka dating samples, leaving the total number of dates used for maximum age estimation of the youngest faulting in the Máze Fault System to 21 (N= 21; i.e., 1 from Trench 5, plus 15 from Trench 7, and plus 5 from Trench 8).

We have as best we could, picked out leaves, twigs, and bark, which we consider most reliable for dating. However, even in these cases young plant remains could possibly be brought to some depth in wet peat due to, e.g., animal tramp or root turnovers, but structures of such events have not been observed, included not in the upper 15-20 cm of the peat, neither at Máze nor at

Fitnajohka. This suggests that the sampled macro plant remains from the surficial peat are *in situ* position and not re-deposited or contaminated from young carbon.

The peat depth and estimated accumulation rate of the undisturbed peat at the western flank of the mire adjacent to the fault scarp at Trench 7, suggest an age of c. 500 years before the present at 20 cm depth (Olsen et al., 2022), and even younger at 15 cm depth, which is the same peat depth as at the eastern flank of the mire where surficial peat there is found disturbed from below from sand wedges injected during the fault event. We consider this as a strong support to the idea of a very young age of the fault event at Máze based on ^{14}C dates of deformed basal part of recent peat at 15-20 cm depth at Trench 7 (Fig. 3; Table 3), and by that also is a strong support for the reliability of the young radiocarbon dates of the fault event from this site.

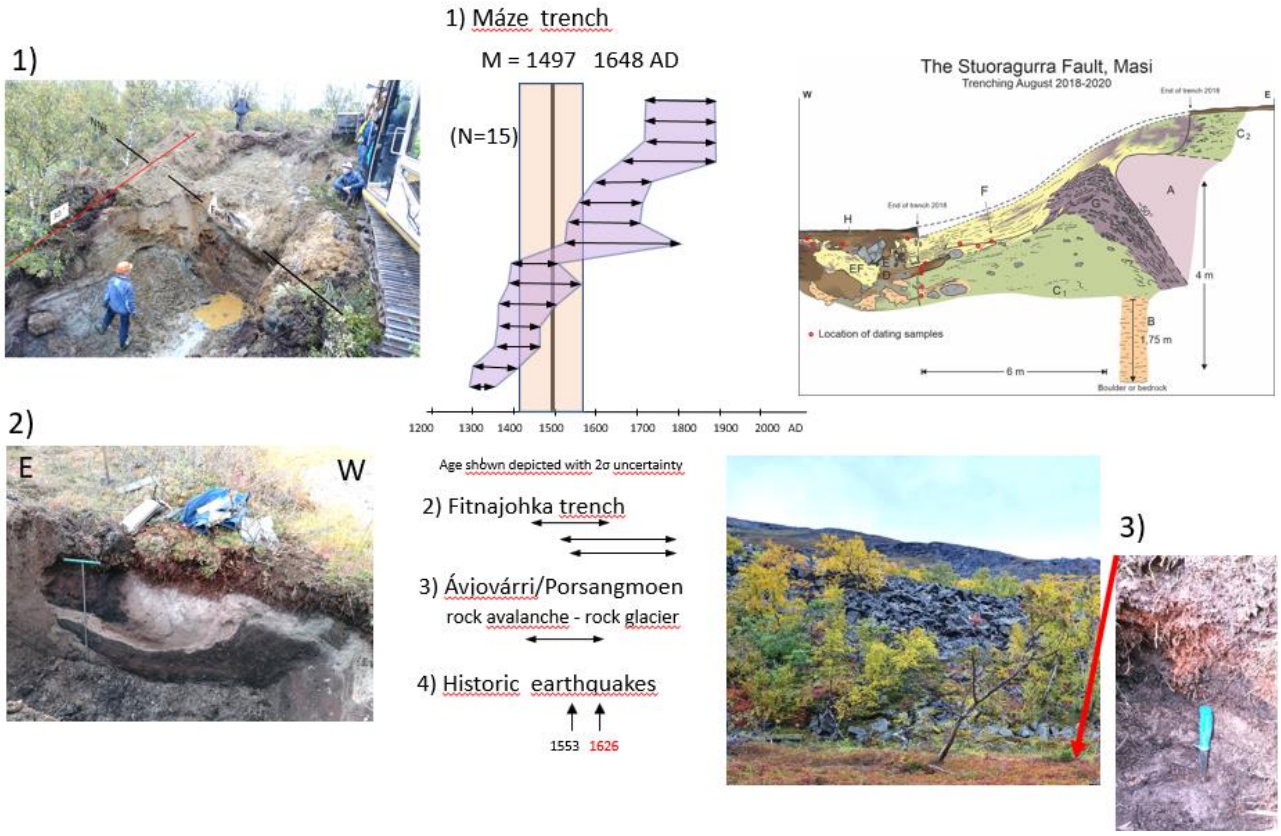

Fig. 27. Results from ^{14}C-dating of macro plant remains in deformed sediments on the footwall of the faults in the SFC at Máze (1) and Fitnajohka (2), and from deformed soil in front of a rock avalanche – rock glacier W of Porsangmoen (3; for location see Fig. 3). Results shown in years AD, and M = mean of max and min ages of the 2σ uncertainty interval shown in the mid column. Two historical earthquakes are also plotted. The youngest of these, at 1626 AD, is considered most relevant associated to the SF due to the dates achieved for estimating a maximum age of the faulting. The diagram is based on data achieved during the 2018-2022 field seasons and accompanying dates. A revised diagram, including field-data and accompanying dates from 2023 are shown in Fig. 28.

The nine segments of the Iešjávri Fault System occur with a spacing of 1–5 km and have a maximum scarp height of 2–3 metres. The length of the individual segments is maximum 2.5 km. Radiocarbon dating of buried organics at Guovžiljohka in the Iešjávri Fault System indicate an age younger than 4.0 cal. kyr BP for the fault event there (Olsen et al., 2022). New data from trenching at Juovssajávrrit (Trench 2) indicate that faulting occurred less than c. 430 years ago also in the northeastern fault system.

A synthesis based on a combination of dates from deformed and buried organic sediments exposed in trenches through the faulting scarps at three dating sites (Máze, Fitnajohka and Juovssajávrrit) in the Stuoragurra Fault Complex is presented in Figs. 27 & 28. Our working hypothesis is now, based on all available data, that the youngest fault event may have occurred at almost the same age in the two (earlier three) separated fault systems of the SFC. At Máze and Fitnajohka in the Máze Fault System the faulting event there occurred less than 430 cal. yr BP, based on 21 ^{14}C dates of plant remains in deformed sediments on the footwall of the fault scarp. At Juovssajávrrit (Figs. 14 & 15) in the Iešjávri Fault System the faulting event most likely occurred less than c. 300-430 cal. yr BP also there (Table 4; nos. 53-54), and the stratigraphy of the sediments in the fault scarp at this site is relatively straight-forward to interpret, i.e., deformed sediments overlain by undeformed soil or peat (Fig. 15). At other sites, e.g., at Máze (Trench 7) and Fitnajoka (Trench 8), the situation was more complex, with both burying of parts of the postglacial peat, and injections into it. We do not know precisely how much of the surficial peat overlying the sandy injections closest to surface, e.g., in the western end of Trench 7 (Máze), which have accumulated after the faulting event. However, it is clearly less than 15-20 cm (Figs. 4D & 6), and the surficial 15-20 cm of the peat represents less than 6-8% of the total c. 2.6 m thick Holocene peat, recorded just outside the western end of Trench 7. These uppermost 15-20 cm thus represents just a few hundred years of accumulation, and, therefore, supports the dating results from this depth level.

We have not been able to find any reports of large-magnitude earthquakes in Finnmark in the 1500s and 1600s. The reason for this may be the sparse population on Finnmarksvidda and long distances (c. 150 km) to the established fishing villages on the islands of Sørøya and Magerøya at the coast in western Finnmark. There are few written accounts from the 1500s in Norway partly because of fires at Akershus castle where the national archive was located.

The first earthquake in North Norway was reported in 1814 in Saltdalen in Nordland (Muir-Wood & Woo, 1987). We thus have 210 years of seismic reporting for northern Norway.

However, several earthquakes were reported from northern Sweden and Finland in the 18th century (Muir-Wood & Woo, 1987). A large-magnitude earthquake was felt throughout northern Finland on 31 December 1758. This event was also reported from

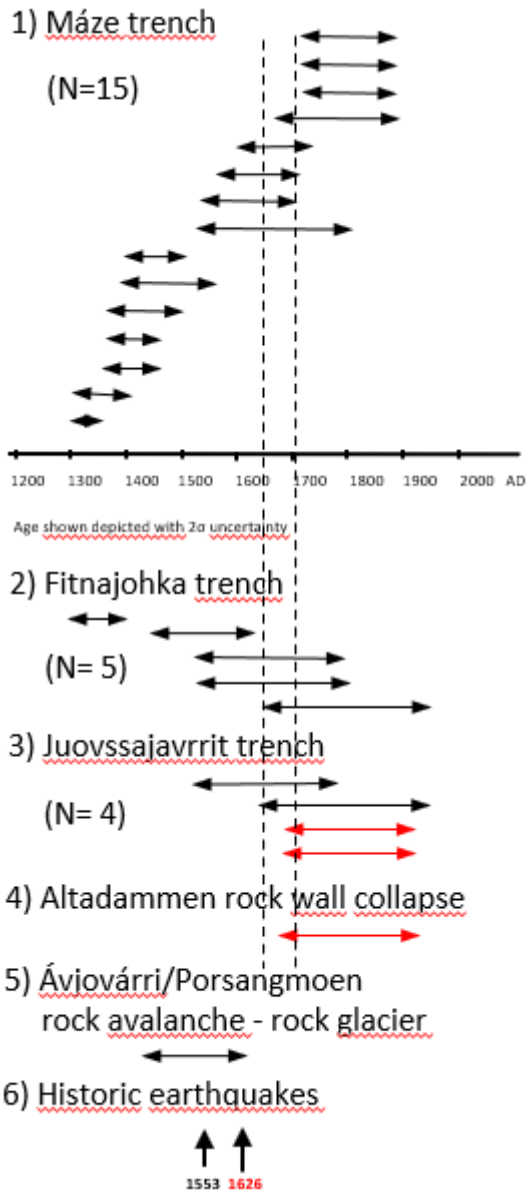

Fig. 28. Age shown in years AD (calendar years) of the Stuoragurra Fault, based on ^{14}C dating of plant remains in deformed sediments in front of the fault scarp at various sites, and exposed by trenching (1, 2, 3). Two examples of rock wall collapse from unstable bedrock slope and rock avalanche, also possibly associated with major earthquakes, are included in the figure (4, 5). 2σ-uncertainty intervals are indicated for maximum ages (black) and minimum ages (red). Two parallel vertical broken lines at c. 1650 and 1700 AD indicate the best estimate of the age (both maximum and minimum) of all faulting, earthquake, rock fall and rock avalanche events included in this diagram. Two historical earthquakes, 1553 and 1626 AD (6), the latter reported e. g. from northern Finland, are indicated in the figure. Based on the uncertainty intervals of our dates both these historical earthquakes are possible candidates associated with the late postglacial Stuoragurra faults. The figure is based on data from field seasons 2018-2023, and accompanying ^{14}C dates, and is modified from Fig. 27.

Karasjok. We think that the sparse reporting of earthquakes from northern Norway may be related to the frequent storms and hurricanes on the coast. Strong shaking may have been misinterpreted as a weather phenomenon. Dwellings mostly consisted of sturdy turf huts that could be easily repaired after damage.

The first churches were built in Altafjorden, Kautokeino and Máze in 1694, 1703 and 1721, respectively. Finnmarksvidda was until 1751 part of Sweden (Nielsen, 1990; Hætta, 2020; Hansen & Olsen, 2022). The priest Johannes Torneaus from Övertorneå in Sweden built the first house in Kautokeino in 1641. The Máze church was, however, built by Norwegians (initiated by Thomas von Westen). The period 1593–1692 was a period of severe witchcraft persecution in Finnmark. In an area with no more than 3,000 inhabitants, 135 people were accused of witchcraft: 91 of them were executed (Lilienskiold, 1695; Sandvik & Winge, 1987; Hagen, 2015; Willumsen, 2010, 2017). The authorities in Vardø were generally looking for people who could manipulate the forces of nature, e.g., cause storms, hurricanes, disease and plague. The Sami people living on Finnmarksvidda and in the neighbouring fjord areas were probably not eager to report strong shaking phenomena. Their knowledge of Norwegian and Danish was most likely rudimentary.

Tatevossian et al. (2011) have localized an earthquake in the area between the Bothnian Bay in Finland and the White Sea in Russia with magnitude 4.7–5.7 on the Richter scale to May or June 1626. The great uncertainty in localization and timing is due to few contemporary reports in Finland, the White Sea area and the Kola Peninsula and the use of different calendars in Russia and Sweden-Finland. If the four reports can be attributed to an earthquake on Finnmarksvidda, such an quake would obviously have been more powerful than the estimated quake at the border between present-day Russia and Finland. The court records (tingbok) for Finnmark (Sandvik & Winge, 1987) are missing one or more pages between 9 June and 29 July 1926. Natural disasters were usually regarded as acts of God (or devil). The Danish-Norwegian king Christian IV suffered a catastrophic defeat at Lutter am Barenberg in Germany between 17 and 27 August 1626 (Heiberg, 2006). The Danish-Norwegian army was almost obliterated and all of Jutland was invaded by German troops. Christian IV was highly superstitious, and we can speculate that he regarded a high-magnitude earthquake that could be felt across most of Norway as a divine sign that he did not honour. He could have avoided critics from the Danish Council of State (Riksrådet) by censoring descriptions of the earthquake.

A total of 16 earthquakes was felt and reported in the eleven-year period 1889–1900 in the Karasjok-Kautokeino area (Muir-Wood & Woo, 1987) indicating a large variation in seismic activity with time in this area.

New and more accurate earthquake records (Keiding et al., 2018; Gregersen et al., 2021), show that the two so-called Iešjávri and Máze fault systems on Finnmarksvidda are part of a 300-kilometre-long Stuoragurra-Merasjärvi fault complex that extends southwards through northern Finland and northern Sweden (Fig. 1). This, and the very young ages now associated to the SFC, suggests that the faulting ages should be attempted dated also for the faults extending further to the southwest in northern Finland and northern Sweden.

Dates representing the minimum age of rock fall and collapse with c. 20 m lowering of the bedrock surface in an unstable mountain slope adjacent to the Alta Dam (Figs. 25 & 26) and maximum age based on deformed organics at the foot in front of a rock avalanche, possibly transformed to a rock glacier during the Little Ice Age, west of Porsangmoen (Fig. 24) are also included in the synthesis (Figs. 27 & 28). These phenomena may have been triggered by strong earthquakes, possible the same ones that are associated with the faulting events.

Soft sediment deformation structures (SSDSs) occur frequently in the faulting sediments, and similar structures have also been recorded in sandy sediments in close-lying locations (Figs. 17, 18 & 19). Formation of s*eismites,* i.e., earthquake induced deformed sediments (Lagerbäck, 1990), with liquefaction features, as also associated to the SSDSs in partially or fully water saturated sediments, require earthquake of at least magnitude 4.5-5 to be produced (e.g., van Loon et al., 2016). Since the SSDSs adjacent to the SFC at Stuoragurra includes also *mosaic sand* (Fig. 17), which represents a high-energy deformation member of SSDSs and seismites (cf. Olsen & Høgaas, 2020), the associated earthquake to produce these structures is probably of at least magnitude 5.

Units of diamicton with breccia structure (unconsolidated fault breccia) adjacent to the fault scarp are produced and injected as wedges into (or onto) the overburden during the faulting events. This was first observed during trenching at Fitnajohka in 1998 (Dehls et al., 2000) and is typically found in several of the trenching sites since Máze 2018 (Trench 7; Figs. 3 & 4D). Fault breccia constitutes a major part of the present unconsolidated overburden. This is recorded in all trenches excavated down to the bedrock, i.e., hanging wall-footwall boundary in the fault scarp area.

Fault clay (gouge) from the Mierojávri–Sværholt shear zone in the Ellajávri area, SSW for Masi, consists mainly of palygorskite and smectite. It is suggested that these minerals were formed by prolonged hydrothermal and diagenetic processes during Cambrian and Ordovician, and this is confirmed by K-Ar dating of the fault clay (460 Ma, Olsen et al., 2022). However, these data do not give reason to suggest an age of the old fault activity in the fault zone. The best data to suggest an age of the older fault activity here is the occurrence of weathered fault gouge, with e.g., kaolinite and vermiculite, at Fitnajohka (Åm, 1994) and lithified fault breccia at all trenched sites where bedrock was reached (7 of 11 sites; the trenching at Guovžiljohka Trench 1, at Juovssajávrrit Trench 2, at Borgagurra Trench 3, and at Fitnajohka Trench 8, Fig. 3, did not reach bedrock). These data altogether imply that the young SFC faulting is just reactivation of an old fault zone.

Large earthquakes in mid-continents such as Australia, Eastern United States, North China and North-western Europe show complex spatiotemporal patterns that do not fit existing seismotectonic models (Clark et al., 2012; Calais et al., 2016; Liu & Stein, 2016). Individual faults tend to fall into long term (thousands of years or longer) dormancy after a cluster of ruptures, whereas large earthquakes seem to roam between widespread faults. This model can also be applied to the postglacial faults within the Lapland Fault Province. The end-glacial faults in the Bay of Bothnia area (e.g., the Lansjärv, Röjnoret and Burträsk faults, Lagerbäck & Sundh, 2008; Fig. 1) could have transferred stress to neighbouring faults and disturbed conditions on distant faults in Finnmark and Finnish Lapland (Olesen et al., 2021). This model can explain the much younger age of the SFC and the northernmost postglacial faults in Finland (Ojala et al., 2019) compared with the Gulf of Bothnia faults in Sweden. It is also compatible with the GIA modelling by Steffen et al. (2014a, b) who predicted faulting along a 45° dipping weakness zone in a prestressed region beneath the centre of the former ice sheet. In such a system, widespread mid-continental faults can accommodate slow tectonic loading from the far field (including ridge push). The most active intraplate seismic zone in Canada is known as the Charlevoix-Kamouraska/Bas-Saint-Laurent seismic zone, where at least five earthquakes of magnitude 6 or greater have occurred over the past 350 years (St-Onge, 2023). Calais et al. (2016) and Craig et al. (2016) argue that the lithosphere can store elastic strain over long timescales, the release of which may be triggered by rapid, local, and transient stress changes caused by erosion, fluid migration or ice loading, resulting in the intermittent occurrence of intraplate seismicity. Liu & Stein (2016) and Calais et al. (2016) conclude that this paradigm shift would make some commonly used concepts such as recurrence intervals and characteristic

earthquakes inadequate in many mid-continental areas. This has significant bearings on the seismic hazard estimates for Fennoscandia and implies that large earthquakes in the order of magnitude 7 can occur today (Olesen et al., 2021).

We speculate that some of the c. 80 earthquakes registered along the postglacial faults in the SFC between 1991 and 2019 (Olesen et al., 2021) may possibly represent aftershocks of a large-magnitude earthquake that occurred less than 500 years ago. Aftershock sequences can according to seismological observations and models (Stein & Liu, 2009) last for centuries in intraplate regions.

The possible different ages of the two (previously three; Olsen et al., 2022) main fault systems in Finnmark are supported by empirical data from historical surface ruptures reported from other faults where distances more than 3–5 km between fault segments often indicate different rupture ages of each fault system (e.g., Wesnousky, 2008). Different periods of postglacial faulting are also evident from age dating of landslides in northern Finland (e.g., Ojala et al., 2018). Radiocarbon age data revealed three episodes of increased landslide formation associated with postglacial faulting, from 11.0 to 9.0 cal. kyr BP, from 7.0 to 5.0 cal. kyr BP, and from 3.0 to 1.0 cal. kyr BP.

Several landslides in the proximity of faults in northern Finland have been found to have occurred over most of the Holocene, as mentioned above. In Norway, we have so far tried to estimate the age of five of the c. 70 recorded landslides less than 20 km from the SFC (Fig. 3). In three of the five cases a large landslide forming the main part of the slide depression occurred during the last deglaciation or shortly after that. In all cases there are also younger, smaller slides represented. It is needed more data to see if clusters of landslide events occur in any age-intervals during the Holocene. Therefore, it is at present premature to discuss in detail whether any of these slides may have been induced by earthquakes and seismicity in intervals, along or close to the SFC, but this possibility seems likely based on the number of such slides close to the SFC.

Ice growth during the Little Ice Age (LIA), which culminated generally in Norway c. 1750 AD, may have led to rock-glacier formation from previous glacial rock accumulations, or rock avalanches and talus, e.g., as west of Porsangmoen (Fig. 24; Olsen et al., 2022). This is possible since such rock glaciers may form and be fully active within a few hundred years (Linge et al., 2020). The maximum age of the normal faulting represented by the Nordmannvikdalen Fault

(Figs. 1 & 29), has been referred to as of late-glacial Younger Dryas age (Bakken, 1983; Tolgensbakk & Sollid, 1988; Dehls et al., 2000; Olsen et al., 2018). However, the age may be

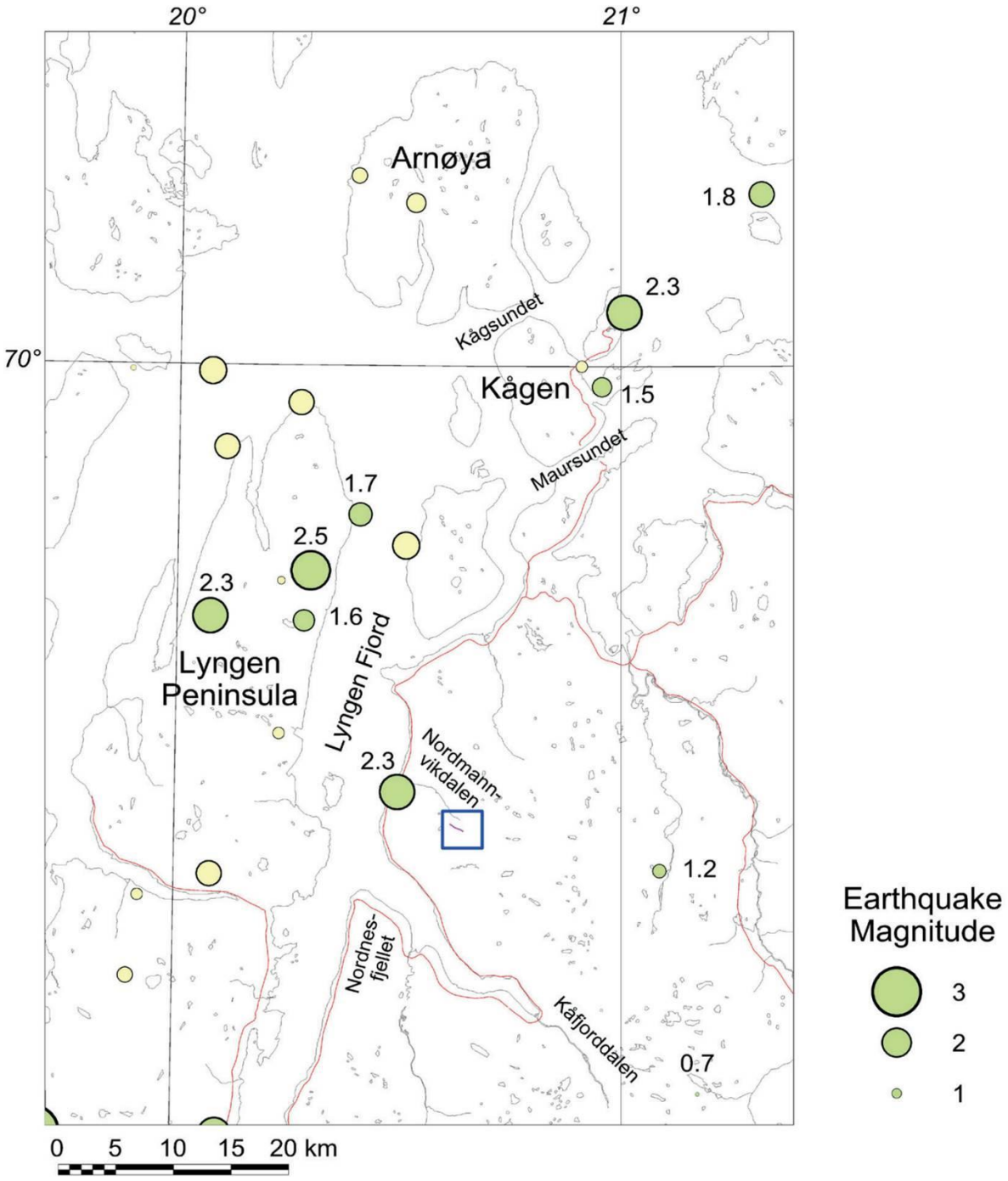

Fig. 29. Map of northern Troms area showing the Nordmannvikdalen Fault as a short black line within the blue framed area (red line and N in Fig. 1) and earthquake magnitudes of recorded modern seismic events in northern Troms-region. Yellow circles show events that have been identified as blasts using an explosion filter. Figure after Olsen et al., 2018.

much younger, and even from the beginning of LIA (i.e., c. 1500-1600 AD), if the fault related fractures along the fault were open for ice growth during LIA, and if the rock-glacier formation crossing the fault line was active during LIA (Olsen et al., 2018). The strong earthquake associated with the Nordmannvikdalen Fault (Table 1) may therefore have occurred almost at the same time, or just a few years or tens of years before the young and strong SFC earthquakes. If this is the case, and since strong earthquakes may trigger rock avalanches, then more effort should be put to estimate the age of previous rock avalanches, e.g., by further ^{10}Be exposure dating of associated rock boulders and rock rupture walls, in a wider region in northern Norway, such as shown from single locations in other areas (e.g., from southern Norway: Wilson et al., 2019). Blikra et al. (2006) suggested that the numerous rock avalanches in North Troms could have been triggered by one or more large-magnitude earthquakes. They concluded that such earthquakes most probable occurred during Younger Dryas (12 800 – 11 600 years ago) since the avalanches had turned into rock-glaciers. They may, however, be much younger.

Further studies are needed to investigate the areas outside the faulting disturbed area (seismic, paleo-seismic, geodesy), to assess potential hazards of large earthquakes in the future and reduce their possible effects. We need to understand the potential for large earthquakes in Norway, particularly in Finnmark and Troms, to mitigate the effects of such events.

The 1929 Grand Banks on the Canadian continental margin earthquake occurred on November 18 and had a moment magnitude of 7.2 (Hanrahan 2004). The earthquake was located in the Atlantic Ocean off the south coast of Newfoundland within the Laurentian Slope Seismic Zone. The tsunami waves had an amplitude of 3–8 metres, and a runup of 13 metres along the Burin Peninsula. It destroyed many south coastal communities, killing 27 people and leaving 1,000 or more homeless.

Our studies also provide important information for ongoing exploration programs offshore northern Norway by estimating the impact of recent uplift and neotectonics that is applicable for understanding subsurface conditions, such as temperature, stress, gas expansion and sealing of reservoirs.

Conclusions

- The 90 km long postglacial Stuorgaurra Fault Complex (SFC) within the SW-NE trending Mierojávri-Sværholt Shear Zone (MSSZ) in the Precambrian of Finnmark, northern

Norway, comprises 29 fault segments, which can be grouped into two major fault systems (The Iešjávri and Máze Fault Systems) separated with a c. 12 km wide gap without any apparent faulting. They were most likely formed during two or more separate earthquakes.

- Trenching across different sections of the faults, including radiocarbon dating of organic material buried in the deformed sediments, reveals a late Holocene age (younger than c. 430 cal. yr BP (Present, P= 1950 AD) in each of the two separate fault systems). This indicates that faulting occurred as much as c. 10 kyr after deglaciation, and is therefore not a direct result of rapid, initial, rebound following deglaciation.
- The dip of the reverse postglacial faults as observed in trenches is 50–55° implying a maximum reverse displacement of approximately 9 m, which together with the length of the fault systems indicate associated earthquakes with a moment magnitude of 6.8-6.9 if just one major fault rupture event happened in each fault system. Less magnitude if more than one fault rupture event occurred in each fault system.
- Units of diamicton with breccia structure (unconsolidated fault breccia) adjacent to the fault scarp is produced and injected as wedges into the overburden during the faulting events and the breccia constitutes a major part of the present unconsolidated overburden. This is recorded in all trenches excavated down to the bedrock, i.e., hanging wall-footwall boundary in the fault scarp area.
- Lithified fault breccia is observed in all trenches reaching bedrock, i.e., in 7 of 11 trenches. This indicates that the young SFC faulting just represents reactivation of an old fault belt, which is as expected due to the location of the SFC within an old shear zone (as mentioned above).
- Palynological data from macro-plant remains from the buried organic matter at Máze reveal a pre-fault vegetation history typical for the early to late Holocene in this area (Olsen et al., 2022).
- Based on aerial photographs and LIDAR data a total of 70 landslides have been identified in relatively flat terrain. They occur mostly in the southern part and within 20 km from the fault scarps, suggesting earthquakes as a major triggering mechanism. Landslides in five locations have been dated, with a major episode during or shortly after deglaciation represented at three sites and small landslides occurring c. 3.3 – 1.7 cal. kyr BP in two sites, and even small to medium sized landslides in modern time at all five sites. In

addition, one medium size and two minor size rock avalanches of supposed late postglacial age are recorded c. 5–13 km from the fault complex.

- A curvilinear c. 600 m long and c. 100 m wide unstable mountain slope occurs along the northwestern shore of the Alta River and c. 3 km from the Alta hydropower dam and c. 15 km from the SFC. A c. 20 m high vertical bedrock wall constitutes the backwall of the unstable mountain slope and indicates a collapse and lowering of the bedrock surface in front of the backwall by this height size, c. 20 m. A ^{14}C dating of peat between that rock fall boulders from the backwall indicates a minimum age of this event to 1683 AD.
- The surprisingly young ages of the SFC earthquakes suggest the need for an evaluation of the geohazards associated to earthquake-triggering of rock avalanches in unstable mountain slopes in western Finnmark and northern Troms.
- Rock avalanches and landslides, potentially triggered by earthquakes, can generate tsunamis in fjords and lakes and constitute the greatest seismic hazard to society in Norway. Such information is therefore of high societal importance for the hazard assessments and mitigating the effects of future large earthquakes in built-up areas and infrastructure.

Acknowledgements

Klemet Johansen Hætta, Nils Erik Eriksen, Nils Peder Eira, Joar Førster, Svein Are Eira, Joar Henning Hætta, Isak Mathis Hætta and Per William Hermansen, as well as the companies Kauto Maskin, Eira Anlegg and Nord Transport (Lakselv) were responsible for the trenching in the field seasons of 2018–2022. Per Edvard Johnsen helped with trenching in 2023. The Geological Survey of Norway (GSN) funded the study in 2018-2022 via the project 378100 ("Glacially Triggered Faulting"; Steffen et al., 2021). In 2023 the funding was given via the project 404400 ("Geophysics of Norway - GON"). Radiocarbon dating was performed by the Poznan Radiocarbon Dating Laboratory, Poland, and by Beta Analytic, USA, via their laboratory in London, England. Irene Lundquist and Cecilie Bjerke drafted some of the figures. We express our gratitude to these persons, companies, dating laboratories and to GSN.

References

Åm, M. 1994: *Mineralogisk og petrologisk karakterisering av vitrings/sleppemateriale fra Stuoragurraforkastningen, Finnmark.* MSc thesis, Norwegian University of Science and Technology, 102 pp.

Andresen A., Agyei-Dwarko, N. Y., Kristoffersen, M. & Hanken, N.M. 2014: A Timanian foreland basin setting for the late Neoproterozoic-early Paleozoic cover sequence (Dividal Group) of northeastern Baltica. *In* Corfu, F., Gasser, D., and Chew, D. M., (eds.): *New perspectives on the Caledonides of Scandinavia and related areas.* Geological Society Special Publications 390, 157–175.

Bakken, A.J.H. 1983: *Nordmannvikdalen kvartærgeologi og geomorfologi.* MSc thesis, University of Oslo, 126 pp.

Bingen, B., Solli, A., Viola, G., Torgersen, E., Sandstad, J.S., Whitehouse, M.J., Rohr, T.S., Ganerød, M. & Nasuti, A. 2015: Geochronology of the Palaeoproterozoic Kautokeino Greenstone Belt, Finnmark, Norway: Tectonic implications in a Fennoscandia context. *Norwegian Journal of Geology*, 95, 365–396, http://dx.doi.org/10.17850/njg95-3-09.

Bjørlykke, A., Rueslåtten, H., van der Lelij, R. & Schönenberger, J. 2022: Ediacaran to early Cambrian weathering of the Kautokeino Greenstone Belt in Finnmark, northern Norway. *Norwegian Journal of Geology, 103*, 25 pp. http://dx.doi.org/10.17850/njg102-3-01

Blikra, L.H., Longva, O., Braathen, A., Anda, E., Dehls, J.F. & Stalsberg, K. 2006: Rock slope failures in Norwegian fjord areas: examples, spatial distribution and temporal pattern. In: Evans, S.G., Mugnozza, G.S., Strom, A. & Hermanns, R.L. (eds.), Landslides from Massive Rock Slope Failure, NATO Science Series 49, Springer, Dordrecht, 475–496. https://doi.org/10.1007/978-1-4020-4037-5-26

Bronk Ramsey, C. 2009: Bayesian analysis of radiocarbon dates. *Radiocarbon* 51(1): 337–360.

Bungum, H. & Lindholm, C. 1997: Seismo- and neotectonics in Finnmark, Kola Peninsula and the southern Barents Sea. Part 2: Seismological analysis and seismotectonics. *Tectonophysics*, 270, 15–28.

Calais, E., Camelbeeck, T., Stein, S., Liu, M. & Craig, T.J. 2016: A new paradigm for large earthquakes in stable continental plate interiors. *Geophysical Research Letters*, 43, 10,621–10,637. http://doi.org/10.1002/2016GL070815

Clark, D., McPherson, A. & Van Dissen, R. 2012: Long-term behaviour of Australian stable continental region (SCR) faults. *Tectonophysics*, 566, 1–30.

Craig, T.J., Calais, E., Fleitout, L., Bollinger, L. & Scotti, O. 2016: Evidence for the release of long-term tectonic strain stored in continental interiors through intraplate earthquakes, *Geophysical Research Letters*, 43, 6826–6836. http://doi.org/10.1002/2016GL069359

Dehls, J., Olesen, O., Olsen, L. & Blikra, L.H. 2000: Neotectonic faulting in northern Norway; the Stuoragurra and Nordmannvikdalen postglacial faults. *Quaternary Science Reviews*, 19, 1445–1460.

Gregersen, S., Lindholm, S., Korja, A., Lund, B., Uski, M., Oinonen, K., Voss, P.H. & Keiding, M. 2021: Seismicity and sources of stress in Fennoscandia. *In* H. Steffen, O. Olesen, and R. Sutinen, (eds.): *Glacially Triggered Faulting.* Cambridge University Press, 177–197.

Hagen, R.B. 2015: *Ved porten til helvete: trolldomsforfølgelse i Finnmark.* Cappelen Damm, Oslo, 307 pp.

Hanrahan, M. 2004: *Tsunami. The Newfoundland tidal wave disaster.* St. John: Flanker Press. 229 pp.

Hansen, L.I. & Olsen, B. 2022: *Samenes historie - fram til 1750,* 2nd. edition. Cappelen Damm, Oslo, 389 pp.

Heiberg, S. 2006: *Christian 4. - en europæisk statsmand.* Gyldendal, Copenhagen, 365 pp.

Henderson, I.H.C., Viola, G. & Nasuti, A. 2015: A new tectonic model for the Kautokeino Greenstone Belt, northern Norway, based on highresolution airborne magnetic data and field structural analysis and implications for mineral potential. *Norwegian Journal of Geology*, 95, 339–363. http://dx.doi.org/10.17850/njg95-3-05

Hestad, H.W. 2021**:** *Statistisk prediksjonsmodellering av steinbreer i Norge.* Masteroppgave, Inst. for geofag, Univ. i Oslo, 1-99.

Hætta, O.M. 2020: Samisk kultur og historie til 1848. Eget forlag. 441 pp.

Keiding, M., Olesen, O. & Dehls, J. 2018: Neotectonic map of Norway and adjacent areas, Scale 1:3 million, Geological Survey of Norway.

Lagerbäck, R. 1990: Late Quaternary faulting and paleoseismicity in northern Fennoscandia, with particular reference to the Lansjärv area, northern Sweden. *Geologiska Föreningens i Stockholm Förhandlingar 112 (4),* 333–354.

Lagerbäck, R. & Sundh, M. 2008: Early Holocene faulting and paleoseismicity in northern Sweden. *Sver. Geol. Unders.*, C836, 80 pp. http://dx.doi.org/10.1016/j.earscirev.2016.09.016

Lilienskiold, H.H. 1695: Trolldom og Ugudelighet i 1600-tallets Finnmark, edited by Rune Blix Hagen & Per Einar Sparboe, Ravnetrykk, Tromsø, 1998, 476 pp.

Lilleøren, **K.S.**, Etzelmüller, B., Rouyet, L., Eiken, T., Slinde, G. & Hilbich, C. 2022: Transitional rock glaciers at sea level in Northern Norway. *Earth Surface Dynamics, 10,* 975-996. https://doi.org/10.5194/esurf-10-975-2022

Liu, M. & Stein, S. 2016: Mid-continental earthquakes: Spatiotemporal occurrences, causes, and hazards. *Earth-Science Reviews*, 162, 364–386.

Linge, H., Nesje, A., Matthews, J.A., Fabel, D. & Yu, S. 2020: Evidence for rapid paraglacial formation of rock glaciers in southern Norway from ^{10}Be surface-exposure dating. *Quaternary Research 97*, 55-70. https://doi.org/10.1017/qua.2020.10

Lund, B., Schmidt, P. & Hieronymus, C. 2009: Stress evolution and fault instability during the Weichselian glacial cycle. *Swedish Nuclear Fuel and Waste Management Co., Stockholm. Technical Report,* TR-09-15, 106 pp.

Lundqvist, J. & Lagerbäck, R. 1976: The Pärve fault: A lateglacial fault in the Precambrian of Swedish Lapland. *Geologiska Föreningens i Stockholm Förhandingar*, 98, 45-51.

Mattila, J., Ojala, A.E.K., Ruskeeniemi, T., Palmu, J.-P., Aaltonen, I., Käpyaho, A., Lindberg, A. & Sutinen, R. 2019: Evidence of multiple slip events on postglacial faults in northern Fennoscandia. *Quaternary Science Reviews,* 215, 242–252. http://doi.org/10.1016/j.quascirev.2019.05.022

Mikko, H., Smith, C., Lund, B., Ask, M.V. & Munier, R. 2015: LiDAR-derived inventory of post-glacial fault scarps in Sweden. *Geol. Fören. Stockh. Förh.,* 137, 334–338.

Moss, E.S. & Ross, Z.E. 2011: Probabilistic fault displacement hazard analysis for reverse faults. *Bull. Seismol. Soc. Am.*, 101, 1542–1553.

Mrope, F.M., Olesen, O., Nasuti, A., Slagstad, T., Gradmann, S. & Gellein, J. in press: Subsurface extent of the Mierojávri–Sværholt shear zone at Masi, Kautokeino Greenstone Belt, Arctic Norway; an integrated geophysical study. *Norwegian Journal of Geology*.

Muir Wood, R. 1989: Extraordinary deglaciation reverse faulting in northern Fennoscandia. *In* Gregersen, S. & Basham, P.W. (eds.): *Earthquakes at NorthAtlantic passive margins: neotectonics and postglacial rebound*. Kluwer Academic Publishers, Dordrecht, The Netherlands, 141–173.

Muir-Wood, R. & Woo, G. 1987: The historical seismicity of the Norwegian continental shelf. Earthquake loading on the Norwegian continental shelf (ELOCS). *NGI/NORSAR/PRINCIPIA Report 2 (1)*, 60 pp and appendices. https://www.geo.uib.no/seismo/REPORTS/Scandinavian_earthquake_archive/

Nielsen, J.P. 1990: *Altas historie, bind 1, de glemte århundrene 1520-1826*. Alta museum, Alta, 397 pp.

Ojala, A.E.K., Markovaara-Koivisto, M., Middleton, M., Ruskeeniemi, T., Mattila, J. & Sutinen, R. 2018: Dating of paleolandslides in western Finnish Lapland. Earth Surf. Process. Landforms. http://doi.org/10.1002/esp.4408

Ojala, A.E.K., Mattila, J., Hämäläinen, J. & Sutinen, R. 2019: Lake sediment evidence of paleoseismicity: Timing and spatial occurrence of late- and postglacial earthquakes in Finland. *Tectonophysics*, 771. http://doi.org/10.1016/j.tecto.2019.228227

Olesen, O. 1988: The Stuoragurra Fault, evidence of neotectonics in the Precambrian of Finnmark, northern Norway. *Norsk Geologisk Tidsskrift*, 68, 107–118.

Olesen, O. & Sandstad, J. 1993: Interpretation of the Proterozoic Kautokeino Greenstone Belt, Finnmark, Norway from combined geophysical and geological data. *Geological Survey of Norway Bulletin*, 425, 43–64.

Olesen, O. & Olsen, L. 2023: Can an earthquake along the Stuoragurra Fault Complex trigger a rock avalanche and tsunami in the Alta hydropower reservoir, Finnmark, northern Norway? *In:* H.A. Nakrem & A.M. Husås (eds.), Abstracts and Proceedings of the Geological Society of Norway 1, 2023, p 71. Vinterkonferansen 2023, January 4th-6th, 2023, https://www.geologi.no/images/Konferanser/Vinterkonferansen2023/Abstract2023.pdf

Olesen, O., Henkel, H., Lile, O.B., Mauring, E. & Rønning, J.S. 1992a: Geophysical investigations of the Stuoragurra postglacial fault, Finnmark, northern Norway. *Journal of Applied Geophysics*, 29, 95–118.

Olesen, O., Henkel, H., Lile, O.B., Mauring, E., Ronning, J.S. & Torsvik, T.H. 1992b: Neotectonics in the Precambrian of Finnmark, northern Norway. *Norsk Geologisk Tidsskrift*, 72, 301–306.

Olesen, O., Blikra, L.H., Braathen, A., Dehls, J.F., Olsen, L., Rise, L., Roberts, D., Riis, F., Faleide, J.I. & Anda, E. 2004: Neotectonic deformation in Norway and its implications: a review. *Norwegian Journal of Geology,* 84, 3–34. ISSN 029-196X.

Olesen, O., Brönner, M., Ebbing, J., Gellein, J., Gernigon, L., Koziel, J., Lauritsen, T., Myklebust, R., Pascal, C., Sand, M., Solheim, D. & Usov, S. 2010: New aeromagnetic and gravity compilations from Norway and adjacent areas – methods and applications. *In* B.A. Vining, S.C. Pickering (eds.): *Petroleum Geology: From mature basins to new frontiers.* Proceedings of the 7th Petroleum Geology Conference. Petroleum Geology Conference series 7, Geological Society of London, 559–586.

Olesen, O., Bungum, H., Lindholm, C., Pascal, C. & Roberts, D. 2013: Neotectonics, seismicity and contemporary stress field in Norway – mechanisms and implications. *In* L. Olsen, O. Fredin, O. Olesen (eds.): *Quaternary Geology of Norway*. Geological Survey of Norway Special Publication, 13, 145–174.

Olesen, O., Olsen, L., Gibbons, S., Ruud, B.O., Høgaas, F., Johansen, T.A. & Kværna, T. 2021: Postglacial faulting in Norway - Large magnitude earthquakes of late Holocene age. *In* H. Steffen, O. Olesen, and R. Sutinen, (eds.): *Glacially Triggered Faulting*. Cambridge University Press, 198–217.

Olsen, L. & Høgaas, F. 2020: «Shaken, not stirred": Mosaic sand – a semi-liquefaction phenomenon originating from strong earthquakes. NGU report 2020.020, 1–32.

Olsen, L., Reite, A., Riiber, K. & Sørensen, E. 1996: Finnmark fylke, kvartærgeologisk kart i målestokk 1:500 000, med beskrivelse. Summary in English. Norges geologiske undersøkelse.

Olsen, L., Olesen, O., Dehls, J. & Tassis, G. 2018: Late–/postglacial age and tectonic origin of the Nordmannvikdalen Fault, northern Norway. *Norwegian Journal of Geology*, 98, 483–500. https://dx.doi.org/10.17850/njg 98-3-09

Olsen, L., Olesen, O. & Høgaas, F. 2020: Dating of the Stuoragurra Fault at Finnmarksvidda, northern Norway. 34th Nordic Geological Winter Meeting January 8th-10th 2020, Oslo,

Norway. *In* H.A. Nakrem, A.M. Husås (eds.): *Abstracts and Proceedings of the Geological Society of Norway*, 1, 2020, 157–158.

Olsen, L., Olesen, O., Høgaas, F., Poliakova, A., Rueslåtten, H., Schönenberger, J., van der Lelij, R., Tassis, G. & Bjørlykke, A. 2022: Trenching and ^{14}C dating of the Stuoragurra Fault Complex in Finnmark, Northern Norway – with some accompanying data included: revised edition. NGU report 2022.010, 1-71.

Palmu, J.-P., Ojala, A.E.K., Ruskeeniemi, T., Sutinen, R. & Mattila, J. 2015: LiDAR DEM detection and classification of postglacial faults and seismically-induced landforms in Finland: a paleoseismic database. *Geol. Fören. Stockh. Förh.*, 137, 344–352.

Reimer, P., Austin, W. E. N , Bard, E., Bayliss, A., Blackwell, P. G., Bronk Ramsay, C., Butzin, M., Cheng, H., Edwards, R. L., Friedrich, M., Grootes, P. M., Guilderson, T. P., Haijdas. I., Heaton, T. J., Bogg, A. G., Hughen, K. A., Kromer, B., Manning, S. W., Muscheler, R., Palmer, J. G., Pearson, C., van der Plicht, J., Reimer, R. W., Richards, D. A., Scott, E. M., Southon, J. R., Turney, C. S. M., Wacker, L., Adolphi, F., Būntgen, U., Capano, M., Fahrni, S., Fogtmann-Schulz, A., Friedrich, R., Köhler, P., Kudak, S., Miyake, F., Olsen,. J., Reinig, F., Sakamoto, M., Sookdeo, A. & Talamo, S. 2020: The IntCal20 Northern Hemisphere radiocarbon age calibration curve (0–55 cal kBP). *Radiocarbon*, 62 (4), pp. 725–757. Published online by Cambridge University Press. https://doi.org/10.1017/RDC.2020.41

Roberts, D., Olesen, O. & Karpuz, M. R. 1997: Seismo- and neotectonics in Finnmark, Kola Peninsula and the southern Barents Sea; Part 1, Geological and neotectonic framework. *Tectonophysics*, 270, 1–13.

Sandvik, H. & Winge, H. 1987: *Tingbok for Finnmark 1620-1633.* Norsk lokalhistorisk institutt, 385 pp.

Siedlecka, A. & Roberts, D. 1996: Finnmark Fylke. Berggrunnsgeologi M 1:500 000. Norges geologiske undersøkelse, Trondheim.

Siedlecka, A., Davidsen, B., Rice, A.H.N. & Townsend, C. 2011: Berggrunnskart; Skoganvarri 2034 IV, M 1:50 000, revidert foreløpig utgave. Norges geologiske undersøkelse, Trondheim.

Sletten, K., Olsen, L. & Blikra, L.H. 2000: Slides in low-gradient areas of Finnmarksvidda. *In* Dehls, J. & Olesen, O. (eds.): *Neotectonics in Norway, Annual Technical Report 1999.* NGU Report 2000.001, 41–42.

Smith, C., Sundh, M. & Mikko, H. 2014: Surficial geologic evidence for early Holocene faulting and seismicity. *Int. J. Earth Sci.*, 103, 1711–1724.

Smith, C.A., Grigull, S. & Mikko, H. 2018: Geomorphic evidence for multiple surface ruptures of the Merasjärvi "postglacial fault", northern Sweden. *Geol. Fören. Stockh. Förh.*, 140. http://doi.org/10.1080/11035897.2018.1492963

Solli, A. 1988: Masi 1933 IV – Bedrock Map. Geological Survey of Norway, Trondheim.

Sollid, J.-L., Andersen, S., Hamre, N., Kjeldsen, O., Salvigsen, O., Sturød, S., Tveitå, T. & Wilhelmsen, A. 1973: Deglaciation of Finnmark, North Norway. *Norsk Geografisk Tidsskrift*, 27, 233–325.

Steffen, R., Steffen, H., Wu, P. & Eaton, D.W. 2014a: Stress and fault parameters affecting fault slip magnitude and activation time during a glacial cycle. *Tectonics*, 33. http://doi.org/10.1002/2013TC003450

Steffen, R., Wu, P., Steffen, H. & Eaton, D.W. 2014b: On the implementation of faults in finite-element glacial isostatic adjustment models. *Computers & Geosciences*, 62, 150–159. http://doi.org/10.1016/j.cageo.2013.06.012

Steffen, H., Olesen, O. & Sutinen, R. (eds.) 2021: Glacially Triggered Faulting. Cambridge University Press, 438 pp. http://doi.org/10.1017/9781108779906

Stein, S. & Liu, M. 2009: Long aftershock sequences within continents and implications for earthquake hazard assessment. *Nature*, 462, 87–89.

St-Onge, G. 2023: Paleoseismicity of a passive and active continental margin at Holocene course. Webinar November 2023, The Canadian Geotechnical Society.

Sutinen, R., Hyvönen, E., Middleton, M. & Ruskeeniemi, T. 2014: Airborne LiDAR detection of postglacial faults and Pulju moraine in Palojärvi, Finnish Lapland. *Glob. Planet. Chang.*, 115, 24–32.

Tatevossian, R.E., Mäntyniemi, P. & Tatevossian, T.N. 2011: On the earthquakes in the Northern Baltic Shield in the spring of 1626. Nat Hazards 57, 133–150. DOI https://doi.org/10.1007/s11069-010-9516-7

Tolgensbakk, J. & Sollid, J.L. 1988: *Kåfjord, kvartærgeologi og geomorfologi 1:50.000, 1634 II.* Geografisk Institutt, Univ. of Oslo.

Townsend, C., Rice, A.H.N. & Mackay, A. 1989: The structure and stratigraphy of the southwestern portion of the Gaissa Thrust Belt and the adjacent Kalak Nappe Complex, N

Norway. *In* R.A. Gayer (Ed.): *The Caledonide Geology of Scandinavia.* Graham and Trotman, London, 111–126.

van Loon, A.J.T., Pisarska-Jamroży, M., Nartišs, M., Krievāns, M. & Soms, J. 2016: Seismites resulting from high-frequency, high-magnitude earthquakes in Latvia caused by Late Glacial glacio-isostatic uplift. *Journal of Palaeogeography 2016, 5(4)*, 363–380.

Wells, D.L. & Coppersmith, K.J. 1994: Empirical relationships among magnitude, rupture length, rupture area, and surface displacement. *Bulletin of the Seismological Society of America*, 84, 974–1002.

Wesnousky, S.G. 2008: Displacement and geometrical characteristics of earthquake surface ruptures: issues and implications for seismic-hazard analysis and the process of earthquake rupture. *Bull. Seismol. Soc. Am.*, 98, 1609–1632.

Willumsen, L.H. 2010: *The witchcraft trials in Finnmark, Northern Norway.* Skald, Leikanger, 418 pp.

Willumsen, L.H. 2017: *Kilder til trolldomsprosessene i Finnmark.* Skald, Leikanger, 320 pp.

Wilson, P., Linge, H., Matthews, J.A., Mourne, R.W. & Olsen, J. 2019: Comparative numerical surface exposure-age dating (^{10}Be and Schmidt hammer) of an early-Holocene rock avalanche at Alstadfjellet, Valldalen, southern Norway. *Geografiska Annaler, Series A, Physical Geography*, *Volume 101*, Issue 4.

Wu, P., Johnston, P. & Lambeck, K. 1999: Postglacial rebound and fault instability in Fennoscandia. *Geophys. J. Int.*, 139, 657–670.

GEOLOGICAL
SURVEY OF
NORWAY

· NGU ·

Geological Survey of Norway
PO Box 6315, Sluppen
N-7491 Trondheim, Norway

Visitor address
Leiv Eirikssons vei 39
7040 Trondheim

Tel (+ 47) 73 90 40 00
E-mail ngu@ngu.no
Web www.ngu.no/en-gb/